Hyper-activation of HUSH complex function by Charcot-Marie-Tooth disease mutation in *MORC2*

Iva A. Tchasovnikarova[1,2†], Richard T. Timms[1†], Christopher H. Douse[3], Rhys C. Roberts[4], Gordon Dougan[5], Robert E. Kingston[2], Yorgo Modis[3] and Paul J. Lehner[1*]

[1]Department of Medicine, Cambridge Institute for Medical Research, Cambridge Biomedical Campus, Cambridge, CB2 0XY, UK

[2]Department of Molecular Biology, Massachusetts General Hospital, and Department of Genetics, Harvard Medical School, Boston, MA 02114, USA

[3]Department of Medicine, University of Cambridge, MRC Laboratory of Molecular Biology, Francis Crick Way, Cambridge Biomedical Campus, Cambridge, CB2 0QH, UK

[4]Department of Clinical Neurosciences, Cambridge Institute for Medical Research, Cambridge Biomedical Campus, Cambridge, CB2 0XY, UK

[5]Wellcome Trust Sanger Institute, Wellcome Trust Genome Campus, Hinxton, Cambridge, CB10 1SA, UK

[†]These authors contributed equally to the work.

[*]Correspondence should be addressed to P.J.L. (pjl30@cam.ac.uk)

Abstract

Dominant mutations in the *MORC2* gene have recently been shown to cause axonal Charcot-Marie-Tooth (CMT) disease, but the cellular function of MORC2 is poorly understood. Here, through a genome-wide CRISPR/Cas9-mediated forward genetic screen, we identify *MORC2* as an essential gene required for epigenetic silencing by the HUSH complex. HUSH recruits MORC2 to target sites in heterochromatin. We exploit a new method – Differential Viral Accessibility (DIVA) – to show that loss of MORC2 results in chromatin decompaction at these target loci, which is concomitant with a loss of H3K9me3 deposition and transcriptional derepression. The ATPase activity of MORC2 is critical for HUSH-mediated silencing, and the most common mutation affecting the ATPase domain found in CMT patients (R252W) hyper-activates HUSH-mediated repression in neuronal cells. These data define a critical role for MORC2 in epigenetic silencing by the HUSH complex and provide a mechanistic basis underpinning the role of *MORC2* mutations in CMT disease.

Keywords: CRISPR/Cas9 forward genetic screen, heterochromatin, H3K9me3, gene silencing, HUSH complex, MORC2, DIVA, chromatin compaction, Charcot-Marie-Tooth disease

Introduction

Chromatin has historically been considered as existing in one of two distinct states: euchromatin or heterochromatin. Euchromatin is generally considered to be gene-rich, transcriptionally-active and associated with an open and accessible conformation, whereas heterochromatin is comparatively gene-poor, highly condensed and refractory to the transcription machinery[1]. Heterochromatin has traditionally been considered as occurring in two distinct flavors: H3K27me3-marked heterochromatin, which is dynamic during development[2], and H3K9me3-marked heterochromatin, which is typically found at repeat-rich regions[3].

A remarkable property of H3K9me3-marked heterochromatin is that it can 'spread' along the arm of a chromosome, which can result in the epigenetic repression of an active gene when it is placed in the vicinity of a heterochromatic domain[4]. This phenomenon gives rise to chromosomal position-effects, a term which refers to the difference in expression when an identical gene is positioned at different sites in the genome[5,6]. We previously exploited the near-haploid KBM7 cell line[7,8] to identify genes required for position-effect variegation in human cells[9]. By isolating a population of cells that displayed epigenetic repression of an integrated green fluorescent protein (GFP) reporter construct and screening for mutants in which this repression was alleviated, we identified four genes that were essential for transgene repression: the histone lysine methyltransferase SETDB1[10], plus the Human Silencing Hub (HUSH) complex subunits TASOR, MPP8 and Periphilin[9]. Through the chromodomain of MPP8[11], HUSH preferentially localizes to genomic loci rich in the repressive histone modification H3K9me3. HUSH-mediated recruitment of the methyltransferase SETDB1 to these sites results in the 'writing' of additional H3K9me3, thereby mediating the spreading of heterochromatin across incoming transgenes[9]. The HUSH

complex also plays a critical role in endogenous heterochromatin maintenance, as deletion of HUSH subunits results in decreased H3K9me3 at hundreds of genomic loci[9] and early embryonic lethality in the mouse[12,13].

HUSH-mediated silencing is achieved through the reading and writing of H3K9me3. However, in order to understand how the deposition of this modification ultimately results in epigenetic repression, knowledge of the full complement of HUSH components is essential. Although our original haploid screen identified the core HUSH complex members and SETDB1, our recent examination of the efficacy of the haploid gene-trap approach suggested that such screens are unlikely to achieve saturation[14]. HUSH-mediated silencing may therefore require additional factors not identified by the original gene-trap screen, and, in support of this idea, we recently identified ATF7IP as an additional factor required for HUSH-mediated repression using a proteomic approach[15].

With the aim of identifying additional genes required for transgene silencing by the HUSH complex, we carried out a genome-wide forward genetic screen using CRISPR/Cas9 technology[16,17]. The CRISPR screen highlighted one additional gene as critical for HUSH-mediated repression: Microchidia CW-type zinc finger 2 (*MORC2*). We show that HUSH recruits MORC2 to heterochromatic sites, where its ATPase activity is required to mediate transgene silencing. Loss of MORC2 results in chromatin decompaction at HUSH target loci, concomitant with a loss of H3K9me3 and transcriptional derepression. Mutations in the ATPase domain of MORC2 have recently been implicated in Charcot-Marie-Tooth (CMT) disease, one of the most frequently inherited neurological disorders. We show that the most common of these mutations (R252W; p.Arg252Trp) results in hyper-activation of HUSH-mediated silencing in neuronal cells. Overall, this study identifies a critical role for MORC2 in

HUSH-mediated repression and provides further insight into the mechanisms underlying HUSH complex function in health and disease.

Results

A genome-wide CRISPR screen identifies an essential role for *MORC2* in HUSH-mediated silencing.

The rapid emergence of CRISPR/Cas9-mediated genome editing technologies has now allowed us to reevaluate the set of genes required for HUSH-mediated transgene silencing (Fig. 1a). The Cas9 nuclease was expressed in the same population of GFP^{dim} KBM7 cells harboring epigenetically-repressed transgenes that we used previously[9], and genome-wide CRISPR-mediated mutagenesis was performed using the GeCKO v2 sgRNA library[18]. Two rounds of fluorescence-activated cell sorting (FACS) were used to enrich for GFP^{bright} cells in which epigenetic repression of the GFP reporter transgene was relieved (Fig. 1b), and sgRNA abundance in the selected GFP^{bright} cells versus the unselected library of mutagenized cells was quantified by Illumina sequencing (Fig. 1c and Supplementary Fig. 1a).

Five genes are known to be critical for HUSH-mediated transgene repression: the three HUSH complex subunits TASOR, MPP8 and Periphilin[9], plus the histone methyltransferase SETDB1[9] and its accessory factor ATF7IP[15]. Three of these positive controls, MPP8, SETDB1 and ATF7IP, were successfully identified by the CRISPR screen; TASOR and Periphilin were not significantly enriched, however, suggesting that the screen failed to reach saturation (Fig. 1c and Supplementary Fig. 1a). Through individual CRISPR/Cas9-mediated gene disruption experiments, we assessed a potential role in transgene silencing for the other most significantly enriched genes (Supplementary Fig. 1b). This revealed an essential role for one additional gene, *MORC2*, a finding which we corroborated in an independent HeLa cell clone harboring a HUSH-repressed GFP reporter construct[9] (Fig. 1d,e). With the

exception of SEL1L, which mediates the degradation of the GFP reporter at the protein level[14], we were unable to validate any of the additional candidate genes (Supplementary Fig. 1b). Therefore, the genome-wide CRISPR screen identified a single novel gene, *MORC2*, as a *bona fide* factor required for HUSH-mediated transgene repression.

The ATPase, CW and coiled-coil domains of MORC2 are essential for HUSH function.

MORC2 is one of four MORC family proteins in humans (MORC1-4)[19]. Although little is known about their functional role in human cells, MORC family proteins have been implicated in epigenetic silencing in plants, worms, and mice[20,21]. *MORC2* encodes a protein containing a GHKL-type ATPase, comprised of the N-terminal ATPase domain plus an associated ribosomal protein S5-like domain, followed by two putative histone binding modules: a CW-type zinc finger and a chromo-like domain (Fig. 2a). To assess which of these domains were required for the function of MORC2 in HUSH-mediated repression, we performed a series of genetic complementation experiments in a MORC2 knockout HeLa clone (Fig. 2b-d and Supplementary Table 1). While exogenous expression of full-length MORC2 or a MORC2 mutant lacking the chromo-like domain resulted in re-repression of the GFP reporter, deletion of both ATPase domains, the S5-like domain alone or the CW-type zinc finger abolished MORC2 activity (Fig. 2e,f). Sequence analysis also predicted the presence of three coiled-coil domains (denoted CC1, CC2 and CC3) (Fig. 2a); deletion of any one of these also abrogated MORC2 function (Fig. 2e,f). Thus, the MORC2 ATPase domain, CW-type zinc finger and coiled-coil domains, but not the chromo-like domain,

appeared to be critical for HUSH-mediated epigenetic repression, with the caveat that although these mutant proteins are expressed in cells (Fig. 2f), we are unable to prove that they are correctly folded.

MORC2 interacts with the HUSH complex.

The genetic association between MORC2 and the HUSH complex suggested that MORC2 might physically interact with HUSH subunits. We were readily able to detect an interaction between a V5 epitope-tagged MORC2 immunoprecipitated from HeLa nuclei and the HUSH subunits TASOR and MPP8 (Fig. 3a). Repeating this assay with a series of V5-tagged N- and C-terminal truncation mutants of MORC2 (Supplementary Table 1) suggested that the second coiled-coil domain (CC2) of MORC2 (residues 548-603) was likely to be essential for this interaction (Supplementary Fig. 2a-c). The interaction between MORC2 and HUSH subunits also occurred in SETDB1 knockout cells (Supplementary Fig. 2d) and deletion of MORC2 did not prevent the interaction between SETDB1 and HUSH (Supplementary Fig. 2e), suggesting independent recruitment of these two potential effector proteins by the HUSH complex. However, like SETDB1, MORC2 did not appear to be a constitutive member of the HUSH complex, as, unlike loss of TASOR, MPP8 or Periphilin[9], loss of MORC2 did not affect the protein levels of HUSH subunits (Supplementary Fig. 2f) nor their localization to chromatin (Supplementary Fig. 2g).

The HUSH complex recruits MORC2 to heterochromatic loci.

To ascertain the physiological relevance of the association between MORC2 and the HUSH complex, we performed chromatin immunoprecipitation followed by deep sequencing (ChIP-seq). Immunoprecipitation of a V5-tagged MORC2 construct expressed in MORC2 knockout cells revealed two modes of MORC2 binding to chromatin (Fig. 3b): a broad distribution across the bodies of genes located in heterochromatin marked by H3K9me3 (Fig. 3c,d and Supplementary Fig. 3a) and a series of discrete peaks at transcriptional start sites (TSSs) (Fig. 3e,f and Supplementary Fig. 3b). Comparing the occupancy of MORC2 with that of endogenous TASOR revealed significant overlap between the heterochromatic regions bound by MORC2 and those occupied by the HUSH complex (Fig. 3c,d). Indeed, MORC2 localization to these heterochromatic sites was dependent on the HUSH complex, as MORC2 occupancy was lost in cells lacking all three HUSH subunits (Fig. 3c,d). Thus, these datasets revealed HUSH-dependent recruitment of MORC2 to heterochromatic loci marked by H3K9me3. The functional relevance of MORC2 recruitment to TSSs remains unclear, but this was not dependent on the HUSH complex (Fig. 3e,f) and did not involve H3K4me3 recognition by the CW domain of MORC2[22] (Supplementary Fig. 4), as has been demonstrated for the CW domains of MORC3 and MORC4[23,24].

In further support of an association between HUSH and MORC2, we also found that the HUSH complex regulated the expression of MORC2. Knockout of HUSH subunits or SETDB1 resulted in an increase in MORC2 expression as measured by quantitative reverse transcription PCR (qRT-PCR) (Supplementary Fig. 2h). In support of the idea that this represented a direct feedback loop, our ChIP-seq data demonstrated both TASOR occupancy and HUSH-dependent recruitment of MORC2 to an H3K9me3-rich site in the *MORC2* promoter (Supplementary Fig. 2i).

MORC2 loss results in chromatin decompaction at HUSH loci.

The catalytic activity of the MORC2 ATPase domain allows MORC2 to remodel nucleosomal templates *in vitro*[25]. Therefore, we hypothesized that ATP hydrolysis by MORC2 might be required to alter chromatin architecture at HUSH target sites *in vivo*. To directly test the functional requirement for MORC2 ATPase activity in HUSH-mediated silencing, we carried out further genetic complementation assays in MORC2 knockout HeLa cells (Fig. 4a). While exogenous expression of wild-type MORC2 restored HUSH function and resulted in the re-repression of the GFP reporter construct, MORC2 variants harboring point mutations in the critical residues of the ATPase domain required for ATP binding (N39A) or hydrolysis (D68A)[25] were non-functional (Fig. 4a,b).

Should the ATPase activity of MORC2 be required to mediate chromatin compaction during HUSH-mediated repression *in vivo*, disruption of *MORC2* should result in a more open chromatin structure at sites of HUSH activity. ATAC-seq is currently a leading method to assay changes in chromatin accessibility *in vivo*[26], but our attempts to exploit this technology to examine potential chromatin decompaction in MORC2 knockout HeLa cells were hampered by a large proportion of contaminating mitochondrial reads[27] and insufficient coverage of the heterochromatic portions of the genome at which HUSH functions (Supplementary Fig. 5a,b). We therefore developed a new approach, Differential Viral Accessibility (DIVA), to examine changes in chromatin accessibility *in vivo*. DIVA is conceptually similar to ATAC-seq, but, rather than identifying transposon integration sites to probe accessible chromatin, DIVA maps the integration sites of exogenous lentiviruses (Fig. 4c and Supplementary Fig.

5c). In contrast to the Tn5 transposase which preferentially integrates near transcriptional start sites, HIV-1-derived lentiviral vectors preferentially target gene bodies[28].

We used DIVA to compare chromatin accessibility in wild-type and MORC2-null HeLa cells. Approximately 20 million independent viral integration sites were mapped in each cell type, and the two datasets were then compared to identify loci exhibiting significantly greater numbers of integrations in the MORC2 knockout cells compared to the parental wild-type cells (Fig. 4c and Supplementary Fig. 5d-g). Considering the genome as a series of 10 kb windows, we identified 278 loci exhibiting chromatin decompaction upon knockout of MORC2 (Fig. 4d and Supplementary Table 2). A large proportion of these loci were heterochromatic sites at which TASOR or MORC2 occupancy was observed by ChIP-seq (Fig. 4e). Notably, many of these loci contained zinc finger (ZNF) genes (Fig. 4f), and, on the ZNF-rich chromosome 19, for example, a striking concordance was observed between the positions of ZNF gene clusters and the loci exhibiting decompaction in MORC2 knockout cells (Fig. 4g). Employing an orthogonal technique based on micrococcal nuclease sensitivity, we validated increased chromatin accessibility in MORC2 knockout cells at four example ZNF loci (Supplementary Fig. 6).

MORC2 knockout results in chromatin decompaction, decreased H3K9me3 and transcriptional derepression.

We also wanted to assess the relationship between MORC2-dependent changes in chromatin accessibility and H3K9me3 deposition. We found that loss of MORC2 in HeLa cells resulted in a decrease in H3K9me3 at the vast majority of loci

exhibiting chromatin decompaction upon MORC2 knockout (Fig. 5a,b and Supplementary Fig. 7a), supporting the idea that chromatin decompaction also results in a concomitant decrease in H3K9me3 levels. Consistent with the functional association between MORC2 and the HUSH complex, 906 of the 918 loci (99%) that we previously found to have lost H3K9me3 upon deletion of either of the three HUSH subunits[9] also showed decreased H3K9me3 levels in MORC2 knockout cells (Fig. 5c). At the vast majority of these sites, H3K9me3 deposition was dependent on the HUSH-associated methyltransferase SETDB1 (Supplementary Fig. 7a,b).

Finally we considered the effect of chromatin decompaction at these sites on gene expression. In addition to a decrease in H3K9me3, we found that decompaction following knockout of MORC2 resulted in an increase in the mean expression level of the 89 genes residing within these loci (Fig. 5d), with 42 genes (47%) displaying >1.2-fold increase in expression. Furthermore, of all 190 genes significantly upregulated upon MORC2 knockout (Fig. 5e), ZNF genes represented the most significantly enriched functional group (Fig. 5f). Consistent with a repressive role for MORC2, the majority of the upregulated genes were direct targets of TASOR and/or MORC2 as assessed by ChIP-seq (Supplementary Fig. 7c,d), and many also exhibited a loss of H3K9me3 and decompaction upon MORC2 knockout (Supplementary Fig. 7e). In contrast, ablation of MORC2 did not result in a global transcriptional change across genes exhibiting HUSH-independent MORC2 occupancy at their TSSs (Supplementary Fig. 7f). Altogether, these data support a model whereby loss of MORC2 results in chromatin decompaction, a loss of SETDB1-mediated H3K9me3 deposition and transcriptional derepression at HUSH target sites.

The R252W CMT mutation in MORC2 hyper-activates HUSH silencing.

Five independent studies have recently reported that dominant mutations in the ATPase domain of MORC2 can cause axonal Charcot-Marie-Tooth (CMT) disease (Fig. 6a)[29–33]. We focused on understanding the functional impact of the most prevalent mutation, an arginine to tryptophan substitution at residue 252 (R252W or p.Arg252Trp in Uniprot: Q9Y6X9-1), which results in a severe axonal form of CMT2[30]. This is the identical mutation to the reported R190W variant of MORC2[29,31,32], which refers to a putative alternative isoform of the protein (Uniprot: Q9Y6X9-2) that lacks 62 amino acids at the N-terminus.

Consistent with the genetic data which suggests a gain-of-function mechanism underlying the pathogenicity of the mutations, MORC2 harboring the R252W mutation did encode a functional protein capable of restoring HUSH-mediated transgene repression in MORC2 knockout HeLa cells (Fig. 6b,c). Moreover, the R252W mutant consistently outperformed the wild-type protein, resulting in enhanced re-repression of the GFP reporter. Indeed, despite being expressed at a lower level that the wild-type protein, the R252W mutation both accelerated the rate of reporter re-repression and enhanced the overall degree of reporter repression observed (Fig. 6d and Supplementary Fig. 8). To verify that this effect was also observed at endogenous genes targeted by HUSH and MORC2, we performed RNA-seq analysis to compare the transcriptome of MORC2 knockout HeLa cells reconstituted with wild-type MORC2 versus the R252W mutant (Supplementary Fig. 9). In agreement with the results from the reporter assays, we found that the R252W mutation resulted in the hyper-repression of MORC2 target genes (Supplementary Fig. 9).

The mutant MORC2 proteins exert a dominant effect in CMT patients, driving the disease phenotype when co-expressed with a wild-type MORC2 allele. Therefore, we considered whether the R252W mutant MORC2 could hyper-repress HUSH target genes when expressed alongside the wild-type protein in MORC2-sufficient cells. First, we found that overexpression of R252W MORC2, but not wild-type, resulted in hyper-repression of a HUSH-responsive "GFP^{dim}" HeLa reporter clone that exhibited weak expression at steady state (Fig. 6e). We then considered whether this effect would also occur at endogenous genes in neuronal cells. Transcriptome analysis of SK-N-SH neuroblastoma cells by RNA-seq (Fig. 6f) showed that overexpression of either wild-type or R252W MORC2 enhanced repression at example HUSH target sites (Fig. 6g); however, this effect was substantially greater with the R252W mutant, despite it being expressed at ~7.5-fold lower levels than the wild-type protein (Fig. 6h). Indeed, of the 91 genes significantly over-repressed by R252W compared to the wild-type protein, 31 (34%) were ZNF genes marked by H3K9me3 (Fig. 6i). Overall these data suggested that the R252W mutation in MORC2 can hyper-activate HUSH-mediated epigenetic repression, resulting in over-repression of HUSH target genes in neuronal cells.

Discussion

The recently-identified HUSH complex is an important regulator of mammalian heterochromatin that is critical for silencing of newly-integrated retroviruses[9] and for normal embryonic development[12,13]. Here, through a genome-wide CRISPR/Cas9-mediated forward genetic screen, we have identified MORC2 as an additional accessory member of the HUSH complex. MORC2 is recruited by the HUSH complex to heterochromatic loci, where its ATPase activity is essential for HUSH-mediated silencing. Exploiting a new method, Differential Viral Accessibility (DIVA), we found that loss of MORC2 resulted in chromatin decompaction at these sites, accompanied by a decrease in H3K9me3 levels and transcriptional derepression. Furthermore, we show that the most commonly identified Charcot-Marie-Tooth disease mutation in the MORC2 ATPase domain, R252W, results in hyper-activation of HUSH-mediated repression at heterochromatic loci.

Previously we identified the HUSH complex through a gene-trap mutagenesis screen in the near-haploid KBM7 human cell line[9]. The rapid emergence of CRISPR/Cas9-mediated genome editing technologies has now allowed us to reexamine the complement of genes required for transgene repression, using a genome-wide library of sgRNAs to create the starting pool of mutant cells. The results of the two screens proved to be complementary, as, although the CRISPR screen failed to identify two of the core HUSH complex subunits detected by the original haploid gene-trap screen, it did reveal an essential role for one additional gene, *MORC2* (Fig. 1). The CRISPR screening technique therefore represents a powerful alternative to the haploid gene-trap approach[14], and, with considerable interest in the design of more efficacious guide RNA libraries[34–36], it is likely that the accuracy of such genome-wide CRISPR screens will continue to improve.

In humans, the MORC protein family comprises four proteins (MORC1-4) plus the more divergent SMCHD1[19]. MORC1 represses transposable elements in the male mouse germ line[21] and MORC2 has been implicated in the response to DNA damage[25], but the molecular function of the mammalian MORC family members remains largely uncharacterized. All MORC proteins share a similar domain architecture, comprising an N-terminal GHKL-type ATPase domain and a CW-type zinc finger, but their functions are likely to be distinct. For example, the inability of the CW-type zinc fingers of MORC1 and MORC2 to recognize methylated H3K4 suggests a different mode of recruitment to chromatin compared to MORC3 and MORC4[22], whilst it is only mutations in MORC2 that are associated with CMT disease[29–33]. A key challenge, therefore, is to elucidate how MORC proteins are recruited to chromatin and to determine their effect on nucleosomal architecture at target sites. Here we demonstrate that HUSH regulates the localization of MORC2 to target sites on chromatin, and that the ATPase activity of MORC2 plays a critical role in altering chromatin architecture at these sites during HUSH-mediated silencing.

The ATPase activity of MORC2 is required to drive nucleosome remodeling *in vitro*[25], and was essential for transgene silencing by the HUSH complex *in vivo* (Fig. 4a,b). Therefore, it followed that the remodeling activity of MORC2 might be required to alter chromatin architecture at these sites to promote gene silencing. Although ATAC-seq has been widely used to study the degree of chromatin “opening” at transcriptional start sites, we found it unsuitable to probe decompaction of heterochromatic regions due to the low proportion of transposon integrations into such sites. Instead of mapping transposon integration sites, DIVA examines the integration preferences of exogenous lentiviruses to probe accessible chromatin. Lentiviruses preferentially target the bodies of genes[28], and indeed our data show that this

approach affords far greater coverage of the heterochromatic sites at which the HUSH complex functions. We therefore anticipate that DIVA may prove a useful approach to interrogate changes in heterochromatin structure *in vivo* in other experimental systems. However DIVA may not be suitable for comparisons between non-isogenic cell lines, where it may be impossible to control for differences in the abundance or activity of other factors influencing viral integration preferences. Furthermore DIVA relies on high-efficiency transduction with lentiviral vectors, which may not be achievable in all cell types, and, compared to the simplicity of ATAC-seq, requires a more involved protocol for the preparation of sequencing libraries to map virus-genome junctions.

Our application of DIVA to compare wild-type and MORC2-null cells revealed that loss of MORC2 resulted in chromatin decompaction at HUSH target sites. The repetitive ZNF gene family represented the most enriched functional group. Many of the ZNF genes are located in clusters covered by high levels of H3K9me3, which also coats other repetitive regions of the genome, including centromeres and tandem repeats. While we did not observe decompaction of these additional repetitive regions upon MORC2 disruption, we do not know how well DIVA will capture these other sites of repressive heterochromatin. Further experiments will be needed to address the specific physiological role of MORC2 with HUSH and SETDB1 in maintaining H3K9me3 across the body of ZNF genes.

The DIVA results suggest that HUSH target loci normally adopt a compact chromatin state which needs to be reversed to alleviate repression. Although repressed genomic regions have canonically been associated with dense chromatin domains that are refractory to the transcription machinery, there may be distinct mechanisms through which such nucleosome compaction is achieved. In particular,

the specific requirement for ATP hydrolysis to drive compaction during HUSH-mediated silencing seems to be distinct from other key repressive complexes. For example, ATP hydrolysis has not been implicated in heterochromatin formation through the SUV39H1-HP1 axis, another major route to H3K9me3-mediated silencing. Compact heterochromatic structures have also been associated with Polycomb-driven repression[37], but again this compaction function does not seem to require an ATP motor and has instead been attributed to a disordered region rich in basic amino acids in PRC1[38]. However, ATP-dependent chromatin remodelers have previously been shown to play an indirect role in transcriptional repression by establishing the appropriate nucleosome spacing for subsequent silencing[39]. For example, the Nucleosome Remodeling Deacetylase (NuRD) complex utilizes the chromatin remodeling function of its CHD subunits to space adjacent nucleosomes, thereby making the histone tails accessible for deacetylation[40]. Therefore, one possibility is that MORC2 is recruited by HUSH to position nucleosomes in a manner that renders the chromatin permissive to transcriptional repression.

The mechanism through which dominant mutations in *MORC2* cause axonal CMT disease[29–33] and severe spinal muscular atrophy (SMA)-like disease[41] is unknown. Given that these patients retain one functional wild-type *MORC2* allele, the disease phenotype is unlikely to result from loss-of-function of the mutant protein. Our data suggest that a gain-of-function effect underlies the phenotype of the MORC2 R252W CMT mutation, which results in hyper-activation of HUSH complex function at both exogenous transgenes and endogenous genomic loci. Indeed, the closely-related MORC1 protein – which represses transposable elements in the male germ line[21] – contains a tryptophan residue at the equivalent position.

Further work will be required to elucidate the biochemical basis underlying the hyper-activation phenotype resulting from the MORC2 R252W mutation. Structural insight into the organization of the MORC2 ATPase domain would be invaluable in assessing the impact of the R252W mutation, and may also guide the rational design of small molecule inhibitors. Inhibition of Hsp90, the prototypical member of the GHKL-family of ATPases, has been successfully achieved using the small molecules geldanamycin and radicicol[42,43], and the latter is also effective against the distantly-related GHKL-family member SMCHD1[44]. Overall, these data suggest that inhibition of the ATPase domain of MORC2 provides an attractive target for the therapeutic modulation of HUSH complex function.

References

1. Wang, J., Lawry, S. T., Cohen, A. L. & Jia, S. Chromosome boundary elements and regulation of heterochromatin spreading. *Cell. Mol. Life Sci.* **71,** 4841–4852 (2014).

2. Margueron, R. & Reinberg, D. The Polycomb complex PRC2 and its mark in life. *Nature* **469,** 343–9 (2011).

3. Becker, J. S., Nicetto, D. & Zaret, K. S. H3K9me3-Dependent Heterochromatin: Barrier to Cell Fate Changes. *Trends Genet.* **32,** 29–41 (2015).

4. Talbert, P. B. & Henikoff, S. Spreading of silent chromatin: inaction at a distance. *Nat. Rev. Genet.* **7,** 793–803 (2006).

5. Schotta, G., Ebert, A., Dorn, R. & Reuter, G. Position-effect variegation and the genetic dissection of chromatin regulation in Drosophila. *Semin. Cell Dev. Biol.* **14,** 67–75 (2003).

6. Akhtar, W. *et al.* Chromatin position effects assayed by thousands of reporters integrated in parallel. *Cell* **154,** 914–27 (2013).

7. Kotecki, M., Reddy, P. S. & Cochran, B. H. Isolation and characterization of a near-haploid human cell line. *Exp. Cell Res.* **252,** 273–80 (1999).

8. Carette, J. E. *et al.* Haploid genetic screens in human cells identify host factors used by pathogens. *Science* **326,** 1231–5 (2009).

9. Tchasovnikarova, I. A. *et al.* Epigenetic silencing by the HUSH complex mediates position-effect variegation in human cells. *Science* **348,** 1481–5 (2015).

10. Schultz, D. C., Ayyanathan, K., Negorev, D., Maul, G. G. & Rauscher, F. J. SETDB1: a novel KAP-1-associated histone H3, lysine 9-specific methyltransferase that contributes to HP1-mediated silencing of euchromatic genes by KRAB zinc-finger proteins. *Genes Dev.* **16,** 919–32 (2002).

11. Kokura, K., Sun, L., Bedford, M. T. & Fang, J. Methyl-H3K9-binding protein MPP8 mediates E-cadherin gene silencing and promotes tumour cell motility and invasion. *EMBO J.* **29,** 3673–87 (2010).

12. Harten, S. K. *et al.* The first mouse mutants of D14Abb1e (Fam208a) show that it is critical for early development. *Mamm. Genome* **25,** 293–303 (2014).

13. Soehn, A. S. *et al.* Periphilin is strongly expressed in the murine nervous system and is indispensable for murine development. *Genesis* **47,** 697–707 (2009).

14. Timms, R. T. *et al.* Genetic dissection of mammalian ERAD through comparative haploid and CRISPR forward genetic screens. *Nat. Commun.* **7,** 11786 (2016).

15. Timms, R. T. *et al.* ATF7IP-Mediated Stabilization of the Histone Methyltransferase SETDB1 Is Essential for Heterochromatin Formation by the HUSH Complex. *Cell Rep.* **17,** 653–659 (2016).

16. Wang, T., Wei, J. J., Sabatini, D. M. & Lander, E. S. Genetic screens in human cells using the CRISPR-Cas9 system. *Science* **343,** 80–4 (2014).

17. Shalem, O. *et al.* Genome-scale CRISPR-Cas9 knockout screening in human cells. *Science* **343,** 84–7 (2014).

18. Sanjana, N. E., Shalem, O. & Zhang, F. Improved vectors and genome-wide libraries for CRISPR screening. *Nat. Methods* **11,** 783–784 (2014).

19. Li, D.-Q., Nair, S. S. & Kumar, R. The MORC family: new epigenetic regulators of transcription and DNA damage response. *Epigenetics* **8,** 685–93 (2013).

20. Moissiard, G. *et al.* MORC family ATPases required for heterochromatin condensation and gene silencing. *Science* **336,** 1448–51 (2012).

21. Pastor, W. A. *et al.* MORC1 represses transposable elements in the mouse male germline. *Nat. Commun.* **5,** 5795 (2014).

22. Liu, Y. *et al.* Family-wide characterization of histone binding abilities of human CW domain containing proteins. *J. Biol. Chem.* **291,** 9000–13 (2016).

23. Liu, Y. *et al.* Structure and function of CW domain containing proteins. *Curr. Protein Pept. Sci.* **17,** 497–506 (2016).

24. Li, S. *et al.* Mouse MORC3 is a GHKL ATPase that localizes to H3K4me3 marked chromatin. *Proc. Natl. Acad. Sci. U. S. A.* **113,** E5108-16 (2016).

25. Li, D.-Q. *et al.* MORC2 signaling integrates phosphorylation-dependent, ATPase-coupled chromatin remodeling during the DNA damage response. *Cell Rep.* **2,** 1657–69 (2012).

26. Buenrostro, J. D., Giresi, P. G., Zaba, L. C., Chang, H. Y. & Greenleaf, W. J. Transposition of native chromatin for fast and sensitive epigenomic profiling of open chromatin, DNA-binding proteins and nucleosome position. *Nat. Methods* **10,** 1213–8 (2013).

27. Wu, J. *et al.* The landscape of accessible chromatin in mammalian preimplantation embryos. *Nature* **534,** 652–7 (2016).

28. Kvaratskhelia, M., Sharma, A., Larue, R. C., Serrao, E. & Engelman, A. Molecular mechanisms of retroviral integration site selection. *Nucleic Acids Res.* **42,** 10209–25 (2014).

29. Sevilla, T. *et al.* Mutations in the MORC2 gene cause axonal Charcot-Marie-Tooth disease. *Brain* **139,** 62–72 (2016).

30. Albulym, O. M. *et al.* MORC2 mutations cause axonal Charcot-Marie-Tooth disease with pyramidal signs. *Ann. Neurol.* **79,** 419–27 (2015).

31. Laššuthová, P. *et al.* Severe axonal Charcot-Marie-Tooth disease with

proximal weakness caused by de novo mutation in the MORC2 gene. *Brain* **139,** e26 (2016).

32. Hyun, Y. S., Hong, Y. Bin, Choi, B.-O. & Chung, K. W. Clinico-genetics in Korean Charcot-Marie-Tooth disease type 2Z with MORC2 mutations. *Brain* **139,** e26 (2016).

33. Zhao, X. *et al.* MORC2 mutations in a cohort of Chinese patients with Charcot-Marie-Tooth disease type 2. *Brain* **139,** e56 (2016).

34. Wang, T. *et al.* Identification and characterization of essential genes in the human genome. *Science (80-.).* **350,** 1096–101 (2015).

35. Doench, J. G. *et al.* Optimized sgRNA design to maximize activity and minimize off-target effects of CRISPR-Cas9. *Nat. Biotechnol.* **34,** 184–191 (2016).

36. Horlbeck, M. A. *et al.* Compact and highly active next-generation libraries for CRISPR-mediated gene repression and activation. *Elife* **5,** (2016).

37. Francis, N. J., Kingston, R. E. & Woodcock, C. L. Chromatin compaction by a polycomb group protein complex. *Science* **306,** 1574–7 (2004).

38. Grau, D. J. *et al.* Compaction of chromatin by diverse Polycomb group proteins requires localized regions of high charge. *Genes Dev.* **25,** 2210–21 (2011).

39. Clapier, C. R. & Cairns, B. R. The biology of chromatin remodeling complexes. *Annu. Rev. Biochem.* **78,** 273–304 (2009).

40. Zhang, Y., LeRoy, G., Seelig, H. P., Lane, W. S. & Reinberg, D. The dermatomyositis-specific autoantigen Mi2 is a component of a complex containing histone deacetylase and nucleosome remodeling activities. *Cell* **95,** 279–89 (1998).

41. Schottmann, G., Wagner, C., Seifert, F., Stenzel, W. & Schuelke, M. MORC2 mutation causes severe spinal muscular atrophy-phenotype, cerebellar atrophy, and diaphragmatic paralysis. *Brain* aww252 (2016). doi:10.1093/brain/aww252

42. Stebbins, C. E. *et al.* Crystal structure of an Hsp90-geldanamycin complex: targeting of a protein chaperone by an antitumor agent. *Cell* **89,** 239–50 (1997).

43. Sharma, S. V, Agatsuma, T. & Nakano, H. Targeting of the protein chaperone, HSP90, by the transformation suppressing agent, radicicol. *Oncogene* **16,** 2639–2645 (1998).

44. Chen, K. *et al.* Genome-wide binding and mechanistic analyses of Smchd1-mediated epigenetic regulation. *Proc. Natl. Acad. Sci. U. S. A.* **112,** E3535-44 (2015).

45. Ran, F. A. *et al.* Genome engineering using the CRISPR-Cas9 system. *Nat. Protoc.* **8,** 2281–308 (2013).

46. Koike-Yusa, H., Li, Y., Tan, E.-P., Velasco-Herrera, M. D. C. & Yusa, K. Genome-wide recessive genetic screening in mammalian cells with a lentiviral CRISPR-guide RNA library. *Nat. Biotechnol.* **32,** 267–73 (2014).

47. Lerdrup, M., Johansen, J. V., Agrawal-Singh, S. & Hansen, K. An interactive environment for agile analysis and visualization of ChIP-sequencing data. *Nat. Struct. Mol. Biol.* **23,** 349–57 (2016).

Author contributions

I.A.T., R.T.T. and P.J.L. conceived the study. Except for the *in vitro* expression and purification experiments which were carried out by C.H.D., I.A.T. and R.T. performed all of the experiments, and, together with Y.M. and P.J.L., analysed the data and wrote the manuscript. G.D., R.C.R. and R.E.K. contributed essential reagents.

Acknowledgements

We are indebted to CIMR core facilities: R. Schulte and his team for FACS, and M. Gratian and M. Bowen for microscopy. We thank S. Andrews for assistance with data analysis using SeqMonk, and S. Kundu and M. Tolstorukov for helpful discussions. This work was supported by the Wellcome Trust, through a Principal Research Fellowship to P.J.L. (101835/Z/13/Z), a Senior Research Fellowship to Y.M. (101908/Z/13/Z), a Sir Henry Wellcome Postdoctoral Fellowship to R.T.T. (201387/Z/16/Z) and a Ph.D studentship to I.A.T, and by the BBSRC, through a Future Leader Fellowship to C.H.D.. I.A.T. is a Damon Runyon Fellow supported by the Damon Runyon Cancer Research Foundation (DRG-2277-16). The CIMR is in receipt of a Wellcome Trust strategic award.

Competing Financial Interests

The authors declare that no competing financial interests exist.

Figure Legends

Figure 1. A genome-wide CRISPR/Cas9-mediated forward genetic screen identifies an essential role for MORC2 in transgene silencing by the HUSH complex. (a,b) A genome-wide CRISPR screen to identify genes required for transgene silencing. Cas9 was expressed in a population of GFP^{dim} KBM7 cells harboring epigenetically repressed transgenes, and genome-wide mutagenesis carried out using the GeCKO v2 sgRNA library (a). Mutant GFP^{bright} cells containing gene disruption events that prevented reporter repression were isolated through two sequential rounds of FACS (b). Black boxes indicate approximate sorting gates. **(c)** Bubble plot illustrating the hits from the screen. All genes targeted by sgRNAs are arranged alphabetically by gene name on the x-axis, with their statistical significance as determined by the RSA algorithm plotted on the y-axis. Bubble size is proportional to the number of active sgRNAs for each gene. Colored bubbles represent validated hits; the HUSH complex subunits TASOR and Periphilin (black) did not reach statistical significance, while SEL1L (orange) is involved in the degradation of the GFP fusion protein[14]. A fully annotated plot is provided in Fig. S1. **(d,e)** MORC2 is required for transgene silencing by the HUSH complex in HeLa cells. CRISPR/Cas9-mediated disruption of MORC2 results in derepression of a HUSH-repressed reporter as measured by flow cytometry (d) or immunofluorescence microscopy (e).

Figure 2. The ATPase, CW and coiled-coil domains of MORC2 are required for HUSH complex function. (a) Schematic representation of the domain structure of MORC2. (CC, predicted coiled-coil; S5, ribosomal S5-like domain; CW, CW-type zinc finger; CD, chromo-like domain) **(b-d)** Generation and validation of MORC2 knockout HeLa cells. A HeLa reporter clone harboring a HUSH-repressed GFP reporter was transfected with a pool of plasmids to express Cas9 and three sgRNAs targeting MORC2. Cells in which the MORC2 gene was disrupted became GFP^+ owing to derepression the GFP reporter and were isolated using FACS (b). The sorted GFP^+ population no longer expressed MORC2 protein as assessed by immunoblot (c). MORC2 knockout single cell clones were then isolated from the GFP^+ sorted population (d). **(e**,**f)** Assessing the domains required for MORC2 function through the genetic complementation of MORC2 knockout cells. Expression of wild-type MORC2 or a MORC2 mutant lacking the chromodomain (ΔCD) in MORC2 knockout cells resulted in re-repression of the GFP reporter transgene. In contrast, MORC2 variants lacking the ATPase, S5, CW or coiled-coil domains were non-functional and did not rescue HUSH-mediated repression (e). Immunoblot validation of expression of the MORC2 deletion mutants (f). All MORC2 variants were expressed with an N-terminal V5 epitope tag followed by an exogenous SV40 nuclear localization signal; detailed sequence information on the composition of the mutants is provided in Supplementary Table 1.

Figure 3. The HUSH complex recruits MORC2 to heterochromatic target sites. **(a)** MORC2 interacts with the HUSH complex. TASOR and MPP8 co-immunoprecipitate with V5-tagged MORC2 expressed in HeLa cells. **(b)** Summary of MORC2 genome occupancy as measured by ChIP-seq. In total 4500 peaks of V5-MORC2 occupancy were detected, the majority of which fell into two categories: binding sites in heterochromatin marked by H3K9me3 (purple; left) and binding sites at transcriptional start sites (green; right). **(c,d)** The HUSH complex recruits MORC2 to heterochromatic sites marked by H3K9me3. TASOR and MORC2 occupancy was observed at a range of sites marked by H3K9me3; MORC2 recruitment at these sites was HUSH-dependent, as V5-MORC2 occupancy was lost in cells lacking all three HUSH subunits[9] (HUSH KO). Three example loci are shown in (c), with summary data across all loci shown in (d). Full ChIP-seq traces including input DNA controls are shown in Supplementary Fig. 3a. **(e,f)** MORC2 recruitment to transcriptional start sites is independent of the HUSH complex. MORC2 occupancy was observed at a large number of transcriptional start sites (TSSs) marked by the H3K4me3 histone modification. This was independent of the HUSH complex, as TASOR occupancy was not observed at these sites and MORC2 occupancy was maintained in cells lacking HUSH subunits. Three example loci are shown in (e), with summary data across all loci shown in (f). Full ChIP-seq traces including input DNA controls are shown in Supplementary Fig. 3b.

Figure 4. Loss of MORC2 results in chromatin decompaction at HUSH target sites. (a,b) ATP hydrolysis by MORC2 is critical for HUSH-mediated transgene repression. Exogenous expression of MORC2 mutants unable to bind (N39A) or hydrolyze (D68A) ATP failed to rescue reporter repression in MORC2 knockout cells (a). Immunoblot validation of expression of the MORC2 point mutants (b). **(c)** Overview of the DIVA methodology, which utilizes large-scale mapping of lentiviral integration sites to probe accessible chromatin. See Supplementary Figure 5c,d for more details. **(d)** Loss of MORC2 results in chromatin decompaction. Scatter plot highlighting the 289 genomic loci (orange) which exhibit increased accessibility in MORC2 knockout cells. Unique lentiviral integration sites mapped to the ZNF772 locus in wild-type and MORC2 knockout cells are shown as an example. DIVA scores for all genomic loci are detailed in Supplementary Table 2. **(e)** The majority of loci exhibiting decompaction upon MORC2 knockout are direct targets of MORC2 and the HUSH complex. Of the 278 decompacted loci, MORC2 and/or TASOR occupancy can be detected at 199 loci (71%). **(f,g)** Loci exhibiting decompaction upon MORC2 knockout are highly enriched for ZNF genes (f), and the decompacted regions across chromosome 19 correspond to sites of ZNF gene clusters (g).

Figure 5. Chromatin decompaction in MORC2 knockout cells is accompanied by a loss of H3K9me3 and transcriptional depression. (a,b) H3K9me3 is lost across the majority of loci exhibiting decompaction upon MORC2 knockout. Of the 278 decompacted loci, a loss of H3K9me3 upon MORC2 knockout in HeLa cells was observed at 220 loci (79%), as measured by ChIP-seq (a). Summary data across all 278 decompacted loci is shown in (b). **(c)** Knockout of MORC2 results in loss of H3K9me3 at the same sites which lose H3K9me3 upon knockout of HUSH subunits. Previously we identified 918 genomic loci in HeLa cells that lose H3K9me3 upon knockout of either TASOR, MPP8 or Periphilin (green dots)[9]; these same loci also exhibited decreased H3K9me3 levels upon knockout of MORC2. **(d,e)** The effect of knockout of MORC2 on the transcriptome. RNA-seq analysis was performed to compare the transcriptome of wild-type and MORC2 knockout HeLa cells. In (d), genes residing in loci exhibiting decompaction in MORC2 knockout cells (n = 89) are highlighted in red; loci exhibiting decompaction also exhibit increased expression as measured by RNA-seq (inset). In (e), all genes exhibiting significantly altered expression between wild-type and MORC2 knockout cells (n = 462; DEseq $P < 0.05$) are highlighted in orange. **(f)** Functional classification of the genes upregulated in MORC2 knockout cells using the DAVID functional annotation tool. Genes upregulated upon MORC2 knockout are highly enriched for ZNF genes.

Figure 6. The R252W mutation in MORC2 associated with Charcot-Marie-Tooth disease hyper-activates HUSH-mediated epigenetic repression. (a) Schematic representation of the mutations associated with CMT affecting the ATPase domain of MORC2. **(b,c)** Assessing the effect of the R252W CMT mutation on MORC2 function through genetic complementation of MORC2 knockout cells. The R252W CMT mutant MORC2 is functional, restoring HUSH-mediated transgene silencing when expressed in MORC2 knockout cells (b). Immunoblot validation of expression of wild-type or R252W mutant MORC2 (c). **(d,e)** The R252W CMT mutation in MORC2 hyper-activates HUSH-mediated transgene silencing in HeLa cells. Time-course of transgene re-repression in MORC2 knockout HeLa cells (d): the R252W MORC2 mutant increases both the rate and overall extent of transgene re-repression. Hyper-repression of a GFP^{dim} HUSH reporter in MORC2-sufficient cells by over-expression of R252W MORC2 (e). **(f)** Schematic representation of the RNA-seq experiment in wild-type SK-N-SH neuroblastoma cells. **(g – i)** Expression of either wild-type MORC2 or the R252W mutant results in hyper-repression of HUSH target genes. RNA-seq in SK-N-SH cells overexpressing either wild-type or R252W MORC2 reveals hyper-repression of example HUSH target genes (g); despite R252W MORC2 being expressed at a much lower level than the wild-type protein (h), this effect was more pronounced with the R252W mutant. In total, 91 genes were hyper-repressed by the R252W mutant (edgeR $P < 0.05$), of which 31 were ZNF genes (i).

Online Methods

Cell culture. HeLa cells were obtained from ECACC and were grown in RPMI 1640 plus 10% fetal calf serum (FCS) and penicillin/streptomycin (100 U/ml); approximate doubling time was 22-23 hours for both wild-type cells all derivative cell lines. KBM7 cells, obtained from Dr. Brent Cochran[7], and HEK 293ET cells, a gift from Dr. Felix Randow, and were cultured in IMDM plus 10% FCS and penicillin/streptomycin (100 U/ml). SK-N-SH cells were a gift from Prof. David Rubinsztein and were grown in DMEM plus 10% FCS and penicillin/streptomycin (100 U/ml); approximate doubling time was 55-60 hours for both wild-type cells and all derivative cell lines. All cell lines were routinely tested for mycoplasma contamination (ATCC Universal Mycoplasma Detection Kit).

Antibodies. The following primary antibodies were used: rabbit α-MORC2 (Bethyl Laboratories, A300-149A used for immunoblot), rabbit α-MORC2 (Santa Cruz Biotechnology, sc-366271, used for immunofluorescence), rabbit α-TASOR (Atlas Antibodies, HPA006735), rabbit α-MPP8 (Proteintech, 16796-1-AP), rabbit α-SETDB1 (Proteintech, 11231-1-AP), mouse α-GFP (Life Technologies, A11120), mouse α-V5 (Abcam, ab27671), rabbit α-V5 (Abcam, ab15828), goat α-Lamin B1 (Santa Cruz, sc-6217), rabbit α-H3K9me3 (Abcam, ab8898), rabbit α-Histone H3 (Biolegend, 601902), rabbit IgG (Cell Signaling, #2729), mouse α-calnexin (AF8, a kind gift from M. Brenner, Harvard Medical School) and mouse α-β-actin (Sigma-Aldrich, A5316). Alexa Fluor 488- and Alexa Fluor 546-conjugated secondary antibodies for immunofluorescence were obtained from Molecular Probes. HRP-conjugated secondary antibodies for immunoblot were obtained from Jackson ImmunoResearch.

CRISPR/Cas9-mediated forward genetic screen. Previously we generated a polyclonal population of GFP^{dim} KBM7 cells harboring epigenetically-repressed transgenes through lentiviral transduction with a vector expressing a GFP-fusion protein from the SFFV LTR promoter (pHRSIN-P_{SFFV}-GFP-HLA-A2). The Cas9 nuclease was stably expressed in this population through lentiviral transduction followed by hygromycin selection (500 µg/ml). One hundred million Cas9-expressing reporter KBM7 cells were transduced with the GeCKO v2 sgRNA library at a multiplicity of infection of ~0.1 and untransduced cells removed from the population through puromycin selection (0.75 µg/ml) commencing 48 hours post-transduction. GFP^{bright} cells resulting from the mutagenesis were enriched by two rounds of FACS, with the first sort taking place 7 days post-mutagenesis and the second sort taking place a further 7 days later. Genomic DNA was extracted (Gentra Puregene Kit) from the selected GFP^{bright} cells after the second sort together with a representative sample of the unsorted mutagenized library that had been grown in parallel for the equivalent amount of time.

The abundance of sgRNAs in each sample was quantified by Illumina sequencing. The variable region of the sgRNAs was amplified in a nested PCR reaction (Q5 High-Fidelity Polymerase, NEB) with forward primers binding the U6 promoter region and reverse primers binding the constant region of the sgRNA. For PCR1, 32 x 100 µl reactions each using 4 µg of DNA were performed for the unselected library sample, and 32 x 100 µl reactions each using 4 µg of DNA were performed for selected cells sample. The products of these reactions were pooled, one-tenth was purified using Agencourt AMPure XP beads (Beckman Coulter), and one-tenth of resulting DNA was used as a template for 12 cycles of PCR2 with Illumina

P5- and P7- adapted primers. Following a further AMPure XP bead purification, PCR products were quantified, pooled and sequenced on an Illumina HiSeq 2500 instrument using 50 bp single-end reads from a custom primer binding immediately upstream of the sgRNA sequence. All primer sequences are detailed in Supplementary Table 3.

The resulting sequence reads were trimmed of the constant portion of the sgRNA using the fastx toolkit, and then aligned to an index of the GeCKO v2 library using Bowtie 2. Uniquely aligning reads were used to generate sgRNA count tables for each sample, which were analyzed further using the RSA algorithm to identify genes significantly enriched for gene disruption events in the selected cells versus the unselected library.

Individual CRISPR/Cas9-mediated gene disruption. Oligonucleotides (Sigma-Aldrich) for top and bottom strands of the sgRNA were phosphorylated with T4 PNK (NEB), annealed by heating to 95ºC followed by slow cooling to room temperature, and then cloned into either the dual Cas9/sgRNA expression vector pSpCas9(BB)-2A-Puro (Addgene #48139, kindly deposited by Dr. Feng Zhang[45]) or the lentiviral sgRNA expression vector pKLV-U6gRNA(BbsI)-PGKpuro2ABFP (Addgene #50946, kindly deposited by Dr. Kosuke Yusa[46]).

Lentiviral expression. Exogenous gene expression was achieved using the expression vectors pHRSIN-P_{SFFV}-GFP-P_{PGK}-Hygro, pHRSIN-P_{SFFV}-GFP-IRES-mCherry-P_{PGK}-Hygro and pHRSIN-P_{SFFV}-GFP-P_{PGK}-Blasto, with the gene of interest

inserted in place of GFP. For lentiviral expression of shRNA constructs, the pHR-SIREN vector was used with hairpins cloned in as BamHI-EcoRI fragments. In all cases, lentivirus was generated through the triple transfection of HEK 293ET cells with the lentiviral transfer vector plus the two packaging plasmids pCMVΔR8.91 and pMD.G using TransIT-293 transfection reagent (Mirus) according to the manufacturer's recommendations. Viral supernatant was typically harvested 48 h post-transfection, cell debris removed using a 0.45 µm filter, and target cells transduced by spin infection at 800 x *g* for 60 min. Transduced HeLa cells were selected with the following drug concentrations: puromycin, 2 µg/ml; hygromycin 50 µg/ml; blasticidin, 3 µg/ml. Transduced SK-N-SH cells were selected using 50 µg/ml hygromycin.

Flow cytometry. Cells were fixed in 1% PFA and analyzed on a FACSCalibur (BD) or a FACSFortessa (BD) instrument. Data was analyzed using FlowJo software. For cell sorting, cells were resuspended in PBS + 2% FCS and FACS was carried on an Influx cell sorter (BD).

Immunofluorescence. HeLa cells were grown overnight on glass coverslips, fixed with the addition of 4% PFA for 10 minutes, permeabilized with 0.5% Triton X-100 for 5 minutes, and then blocked for at least 30 min using 4% BSA dissolved in PBS + 0.1% Tween-20 (PBS-T). The primary antibody was diluted in 40 µl of blocking solution and was applied for 1 h, and, following five washes in PBS-T, fluorophore-conjugated secondary antibody (Molecular Probes) was applied for 45 min in the same way. Following a further five washes in PBS-T and a final rinse in distilled water, coverslips

were mounted in 4 µl ProLong Gold Antifade Mountant with DAPI (Thermo Fisher Scientific) and imaged using a Nikon LSM880 laser scanning confocal microscope (Zeiss). Images were processed using Adobe Photoshop (Adobe, CA) or GIMP 2.

Co-immunoprecipitation. Cells were washed once in PBS and then lysed in cell lysis buffer (0.5% IGEPAL, 85 mM KCl and 10 mM HEPES in distilled water). Nuclei were harvested by centrifugation at 800 x *g* for 5 minutes at 4ºC, and then lysed in nuclear lysis buffer (1% IGEPAL plus 1:100 Benzonase in TBS). Insoluble nuclear material was removed by centrifugation (10,000 x *g* for 5 minutes at 4ºC) and then the supernatant was pre-cleared with protein G magnetic beads (Thermo Fisher Scientific) for 1 h at 4°C. Immunoprecipitation was performed by adding 1 µg of antibody and protein G magnetic beads for 2 h at 4°C, and, following three washes of the beads in lysis buffer, samples were eluted in SDS sample buffer.

Immunoblotting. Cells were lysed in 1% SDS plus 1:100 Benzonase (Sigma-Aldrich) for 20 minutes at room temperature, and then heated to 70°C in SDS sample buffer for 10 min. Following separation by SDS-PAGE, proteins were transferred to a PVDF membrane (Millipore) which was then blocked in 5% milk in PBS + 0.2% Tween-20. Membranes were probed overnight with the indicated antibodies, washed three times PBS + 0.2% Tween-20, and then incubated with HRP-conjugated secondary antibodies (Jackson ImmunoResearch) for 45 minutes at room temperature. Reactive bands were visualized using SuperSignal West Pico or West Dura (Thermo Fisher Scientific). All blots presented in the figures have been cropped; the original uncropped images can be found in Supplementary Figure 10.

Subcellular fractionation. One million cells were washed in PBS and then again in Buffer A (10 mM HEPES, 1.5 mM $MgCl_2$, 10 mM KCl, 0.5 mM DTT and an EDTA-free protease inhibitor cocktail tablet (Roche)). The cells were then lysed upon resuspension in Buffer A plus 0.1% (v/v) IGEPAL on ice for 10 min. Nuclei were pelleted by centrifugation (1400 x *g* for 4 min at 4°C) and the supernatant, which contains the cytosolic fraction, was collected. The nuclear pellet was resuspended in Buffer B (20 mM HEPES, 1.5 mM $MgCl_2$, 300 mM NaCl, 0.5 mM DTT, 25% v/v glycerol, 0.2 mM EDTA and an EDTA-free protease inhibitor cocktail tablet) for 10 min on ice, and, following centrifugation at 1700 x *g* for 4 min at 4°C, the supernatant (containing the nucleosolic fraction) was removed. The insoluble pellet, constituting the chromatin fraction, was subsequently solubilized in 1% SDS plus 1:100 Benzonase for 20 min at room temperature.

ChIP-seq. Cells were washed once in PBS, resuspended in growth medium, and then cross-linked in 1% formaldehyde for 10 min. The reaction was quenched by adding glycine to a final concentration of 0.125 M for 5 min before the cells were lysed in cell lysis solution (1 mM HEPES, 85 mM KCl, 0.5% IGEPAL). Nuclei were pelleted by centrifugation, and then resuspended in nuclear lysis solution (5 mM Tris, 10 mM EDTA, 1% SDS) for 10 min. The chromatin was sheared using a Bioruptor (Diagenode; high power, 20 cycles of 30 s on, 30 s off) to obtain a mean fragment size of ~300 bp. Insoluble material was removed by centrifugation. The chromatin solution was pre-cleared with protein A sepharose (Sigma-Aldrich) and then immunoprecipitated overnight using 5 µg primary antibody and protein A sepharose, or, for V5-MORC2, anti-V5 agarose affinity gel (Sigma-Aldrich, A7345). The next day the beads were washed a total of five times, and then bound protein-DNA complexes

eluted in 150 mM $NaHCO_3$ and 1% SDS. Cross-links were reversed by overnight incubation at 67ºC with 0.3 M NaCl and RNaseA. Proteinase K was then added and the samples incubated for 2 h at 45ºC, and then the DNA was purified using a spin column (Qiagen PCR purification kit). Illumina sequencing libraries were produced from this material using the TruSeq ChIP sample prep kit (Illumina), and 50 bp single-end reads generated on a HiSeq 2500 instrument. Reads were aligned to the human genome (GRCh37) using Bowtie 2, and reads with a MAPQ score >10 were imported into SeqMonk and EaSeq[47] for further analysis. V5-MORC2 binding sites were identified using the implementation of the MACS peak caller in SeqMonk (windows size = 300 bp; p-value < 0.0001) and the resulting 4500 peaks were centered and plotted using the Average Signal Tracks tool in EaSeq. H3K4me3 ChIP-seq data generated by the Bernstein laboratory was downloaded from the ENCODE project (ENCSR000AOF).

qRT-PCR. RNA was prepared using the RNeasy Plus kit (Qiagen) and converted into cDNA using Super RT reverse transcriptase (HT Biotechnology) and a poly(dT) primer. Quantification by qPCR was performed on an ABI 7500 Real Time PCR System (Applied Biosystems) using SYBR green PCR mastermix (Life Technologies) in a final reaction volume of 25 µl. Thermal cycling parameters were: 50°C for 2 min; 95°C for 5 min; 40 cycles of 95°C for 15 s and 58°C for 1 min. Error bars represent the standard deviation of at least three technical replicates. Primer sequences are detailed in Supplementary Table 3.

Expression and purification of the CW domain of MORC2. A synthetic, *E. coli* codon-optimized DNA construct (IDT) encoding the MORC2 CW domain (residues 490-546) plus a C-terminal FLAG tag was cloned into the expression vector pET-28a-N-His-SUMO between the BamHI and NotI restriction sites for production of the N-terminally His-SUMO-tagged protein product. Protein was produced in *E. coli* BL21(DE3) cells through overnight incubation at 18 ºC with shaking at 220 rpm following induction with 200 µM IPTG. Cell pellets were resuspended in 30 ml lysis buffer (50 mM Tris-HCl, 500 mM NaCl, 10 mM imidazole, 0.1 mM $ZnSO_4$, 1 mM DTT, 1x Complete EDTA-free protease inhibitors, pH 8.0), flash frozen in liquid nitrogen and stored at -80 ºC.

Pellets were thawed and further lysed by sonication on ice, before clarification by centrifugation (45 min, 40,000 x *g*, 4ºC). The resulting His-SUMO-CW-FLAG-containing supernatant was subjected to immobilized Ni-NTA affinity chromatography with wash (50 mM Tris.HCl, 500 mM NaCl, 10 mM imidazole, 0.1 mM $ZnSO_4$, 1 mM DTT, pH 8.0) and elution (50 mM Tris.HCl, 500 mM NaCl, 300 mM imidazole, 0.1 mM $ZnSO_4$, 1 mM DTT, pH 8.0) buffers, and then desalted using a Bio-Rad Econo-Pac 10DG column into cleavage buffer (20 mM HEPES, 150 mM NaCl, 0.1 mM $ZnSO_4$, 1 mM DTT, pH 7.4). The His-SUMO tag was cleaved from the protein by the addition of His-tagged SENP1 protease (1:10 w/w) for 18 h on ice. Subtractive immobilized Ni-NTA affinity chromatography was then used to deplete the tagged protease and the free His-SUMO tag, and the protein was further purified by size exclusion chromatography on a Superdex 75 (10/300) column in a buffer containing 20 mM HEPES, 200 mM NaCl, 0.1 mM $ZnSO_4$, 1 mM TCEP, pH 7.3. The mass of the intact, pure proteins were confirmed using a Waters Xevo G2 Q-ToF mass spectrometer.

Differential Viral Accessibility (DIVA). Six million wild-type and MORC2 knockout HeLa cells were seeded at a density of $1x10^6$ cells per well of a 6-well plate, and transduced on successive days with the lentiviral vector pHRSIN-P_{SFFV}-mCherry-WPRE (encoding the mCherry fluorescent protein driven by the spleen focus-forming virus LTR promoter) at high multiplicity of infection such that ~100% of the cells were $mCherry^+$. One day after the second transduction genomic DNA was extracted (Gentra Puregene Kit) and digested overnight with NlaIII (NEB). The distribution of NlaIII sites in the lentiviral vector is such that DNA fragments smaller than ~1.8 kb cannot contain viral-genome junctions; large fragments were therefore enriched through a size-selection step using a 0.5x Agencourt AMPure XP bead clean-up (Beckman Coulter). An annealed dsDNA adaptor with an NlaIII-compatible overhang was then ligated onto the ends of the genomic DNA fragments using T4 DNA Ligase (NEB) overnight at 16°C, and the ligated products purified through a further AMPure bead clean-up. Virus-genome junctions were then amplified in 200 cycles of a linear PCR reaction using Accuprime Taq (Thermo Fisher Scientific) using a biotinylated primer binding the just upstream of the 5' LTR in the integrated provirus, and the resulting products were annealed to streptavidin-coated M-280 dynabeads (Thermo Fisher Scientific). Following 5 x 10 minute washes with PBS + 0.1% Tween-20, virus-genome junctions were amplified through 12 cycles of on-bead exponential PCR reaction with an Illumina P5-adapted primer binding the proviral 5'LTR and a P7-adapted reverse primer binding the splinkerette adaptor. After a final AMPure XP clean-up, PCR products were quantified, pooled and sequenced on an Illumina HiSeq2500 instrument generating 50 bp single-end reads from a custom primer annealing to the extreme end of the proviral 5' LTR. All oligonucleotide sequences are detailed in Supplementary Table 3.

The resulting sequence reads were trimmed of adaptor sequences using the fastx toolkit and aligned to the human genome (hg19) using Bowtie 2. Reads with a MAPQ score > 10 were imported into SeqMonk and converted into a set of unique points of integration. The Intensity Difference Filter in Seqmonk was used to identify 10 kb genomic windows (overlapping by 5 kb) significantly enriched for lentiviral integration sites in MORC2 knockout cells versus the parental wild-type cells; individual loci were only considered to exhibit decompaction if at least two adjacent windows reached statistical significance. Full data for all genomic loci is detailed in Supplementary Table 2.

Micrococcal nuclease accessibility assay. Wild-type and MORC2 knockout HeLa cells were washed once in PBS, resuspended in growth medium, and then cross-linked by the addition of 1% formaldehyde for 10 min. The reaction was quenched by addition of glycine to a final concentration of 0.125 M for 5 min. The cells were then lysed in cell lysis solution (1 mM HEPES, 85 mM KCl, 0.5% IGEPAL) and nuclei pelleted by centrifugation (800 x *g*, 5 min, 4°C). The nuclei (5 x 10^5 per reaction) were then resuspended in micrococcal nuclease buffer supplemented with BSA (NEB), and chromatin digested by the addition of 2 units of micrococcal nuclease (NEB) for 30 min at 37°C. EDTA was added to a final concentration of 45 mM to stop the reaction. Nuclei were then lysed in 1% SDS, RNA digested with RNaseA (37°C for 30 min) and cross-links reversed overnight at 65°C. Proteins were then digested with proteinase K (37°C for 2 h) and DNA isolated by phenol-chloroform extraction followed by ethanol precipitation. Size-selection of the digested DNA was achieved using SPRIselect beads (Beckman Coulter) using 0.6 volumes of beads. The bound fraction contained large fragments (>~1000bp); the supernatant containing unbound fragments

(<~1000bp) was removed and subsequently purified by the addition of an extra 1 volume of beads. The amount of DNA from target loci in the accessible and inaccessible fractions versus the pre-size-selected starting material was measured by qPCR performed on a CFX96 Touch Real-Time PCR machine (Bio-Rad) using iTaq Universal SYBR Green Supermix (Bio-Rad) in a final reaction volume of 25 µl. Thermal cycling parameters were: 50°C for 2 min; 95°C for 5 min; 40 cycles of 95°C for 15 s and 58°C for 1 min. Error bars represent the standard deviation of at least three technical replicates. Primer sequences are detailed in Supplementary Table 3.

RNA-seq. Total RNA was extracted using the miRNEasy kit (Qiagen) as per the manufacturer's instructions and multiplexed Illumina sequencing libraries were prepared using the TruSeq Stranded Total RNA Library Prep Kit (Illumina). For the comparison between wild-type and MORC2 knockout HeLa cells, ribosomal RNA was depleted using the Ribo-Zero Gold rRNA Removal Kit (Epicentre) and 150 bp paired-end reads were generated on an Illumina HiSeq2500 instrument. For all comparisons between wild-type and R252W MORC2, polyA$^+$ RNA was sequenced on an Illumina HiSeq2500 instrument using 50 bp single-end reads. Sequence reads were aligned to the human genome (GRCh37) using HISAT2. Mapped reads with a MAPQ score >40 were imported into SeqMonk and further analyzed using the RNA-seq quantitation pipeline followed by DEseq2 or edgeR analysis.

Statistics. No statistical methods were used to predetermine sample size. Experiments were not randomized and the experimenters were not blinded to the outcome. Genes significantly enriched for inactivating mutations in the CRISPR screen

were evaluated using the RSA algorithm comparing the frequency of sgRNAs in the GFP^{bright} selected population versus the unselected mutangenized pool. All qRT-PCR data is represented as the mean +/- standard deviation of at least three technical replicates, and the data are representative of at least two independent experiments. For the RNA-seq data presented in Fig. 5e, three independent MORC2 knockout clones were used; genes exhibiting significantly altered expression in MORC2 knockout cells were identified using the implementation of DEseq2 in Seqmonk ($P < 0.05$). For the RNA-seq data presented in Fig. 6g-i, cells were transduced in triplicate with lentiviral vectors to express either wild-type or R252W mutant MORC2; genes exhibiting significantly reduced expression upon expression of the R252W mutant as compared to wild-type MORC2 were identified using the implementation of edgeR in Seqmonk ($P < 0.05$).

Data availability. The sequence data from the CRISPR/Cas9 forward genetic screen, ChIP-seq, DIVA and RNA-seq experiments that support the findings of this study have been deposited in GEO with the primary accession code GSE95480.

Figure 1

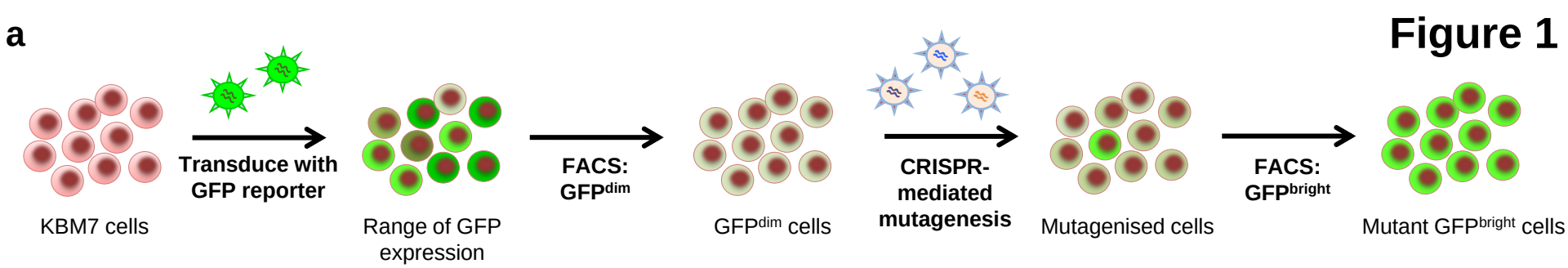
a
KBM7 cells
Transduce with GFP reporter
Range of GFP expression
FACS: GFPdim
GFPdim cells
CRISPR-mediated mutagenesis
Mutagenised cells
FACS: GFPbright
Mutant GFPbright cells

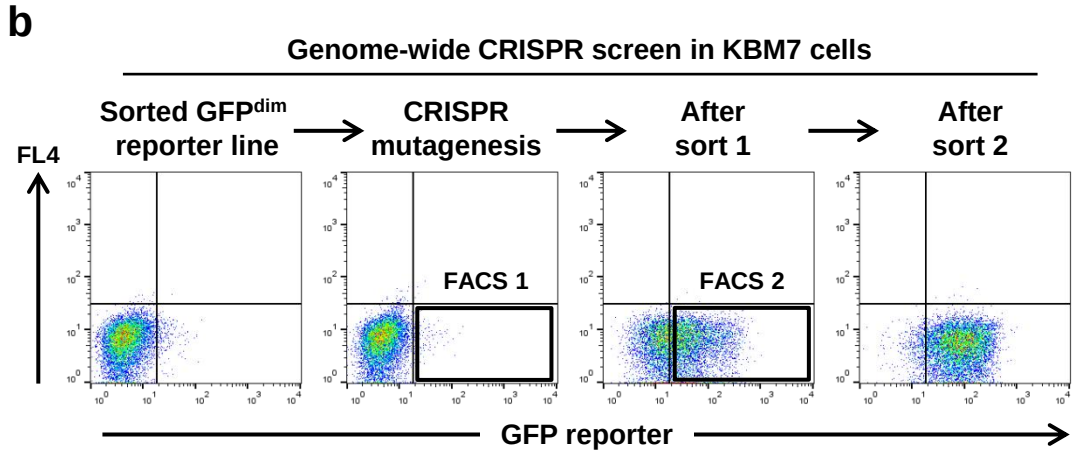
b
Genome-wide CRISPR screen in KBM7 cells
Sorted GFPdim reporter line
CRISPR mutagenesis
After sort 1
After sort 2
FL4
FACS 1
FACS 2
GFP reporter

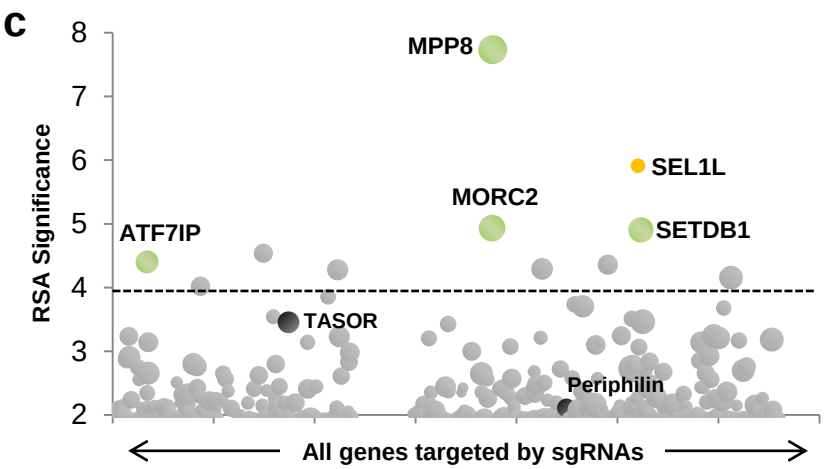
c
RSA Significance
MPP8
SEL1L
MORC2
SETDB1
ATF7IP
TASOR
Periphilin
All genes targeted by sgRNAs

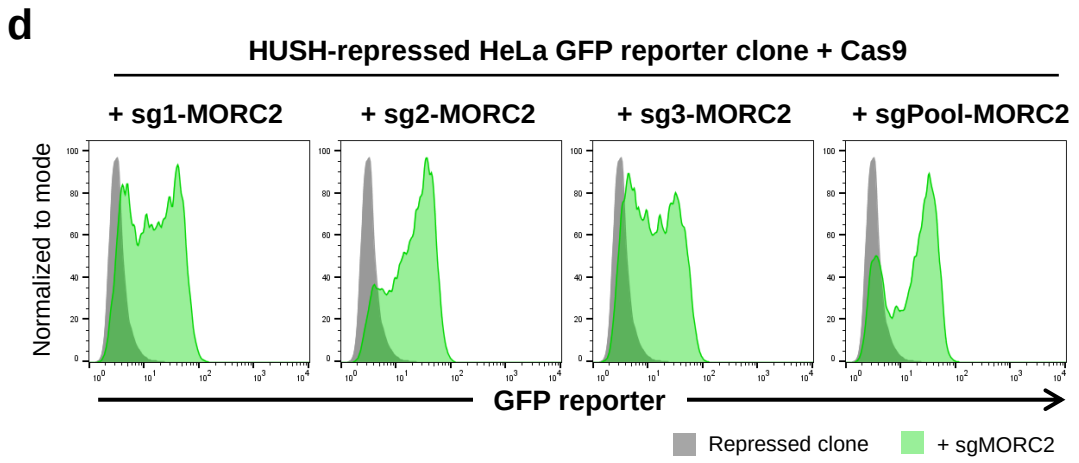
d
HUSH-repressed HeLa GFP reporter clone + Cas9
+ sg1-MORC2
+ sg2-MORC2
+ sg3-MORC2
+ sgPool-MORC2
Normalized to mode
GFP reporter
Repressed clone
+ sgMORC2

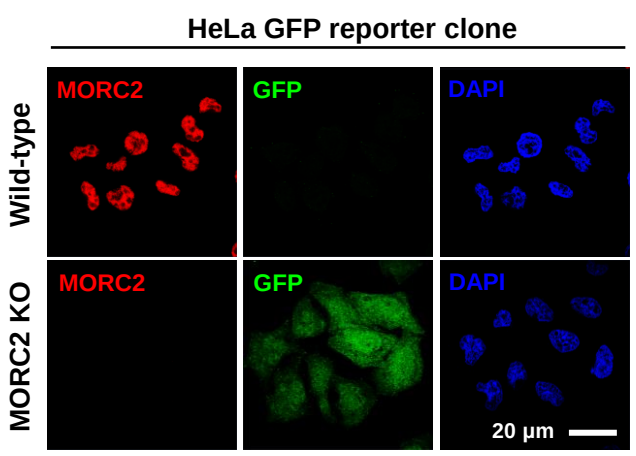
e
HeLa GFP reporter clone
Wild-type
MORC2 KO
MORC2
GFP
DAPI
20 µm

Figure 2

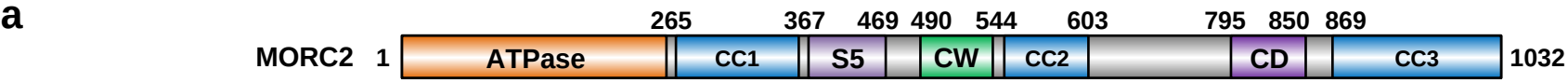
a
MORC2
1
265
367
469
490
544
603
795
850
869
1032
ATPase
CC1
S5
CW
CC2
CD
CC3

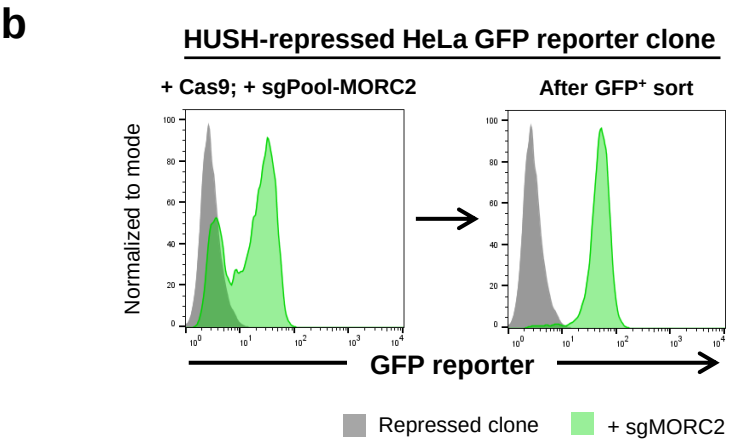
b
HUSH-repressed HeLa GFP reporter clone
+ Cas9; + sgPool-MORC2
After GFP+ sort
Normalized to mode
GFP reporter
Repressed clone
+ sgMORC2

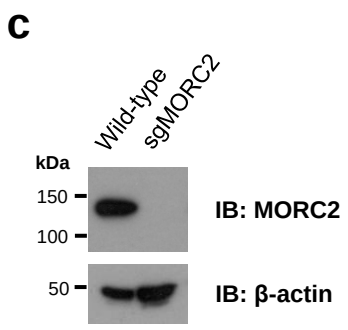
c
Wild-type
sgMORC2
kDa
150
100
50
IB: MORC2
IB: β-actin

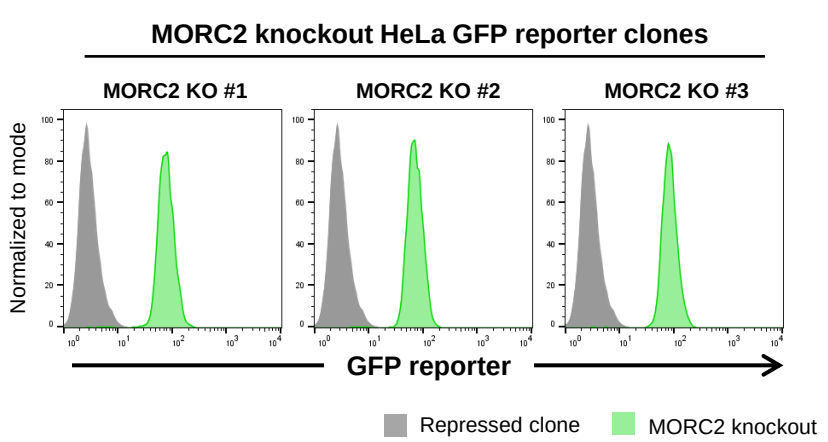
d
MORC2 knockout HeLa GFP reporter clones
MORC2 KO #1
MORC2 KO #2
MORC2 KO #3
Normalized to mode
GFP reporter
Repressed clone
MORC2 knockout

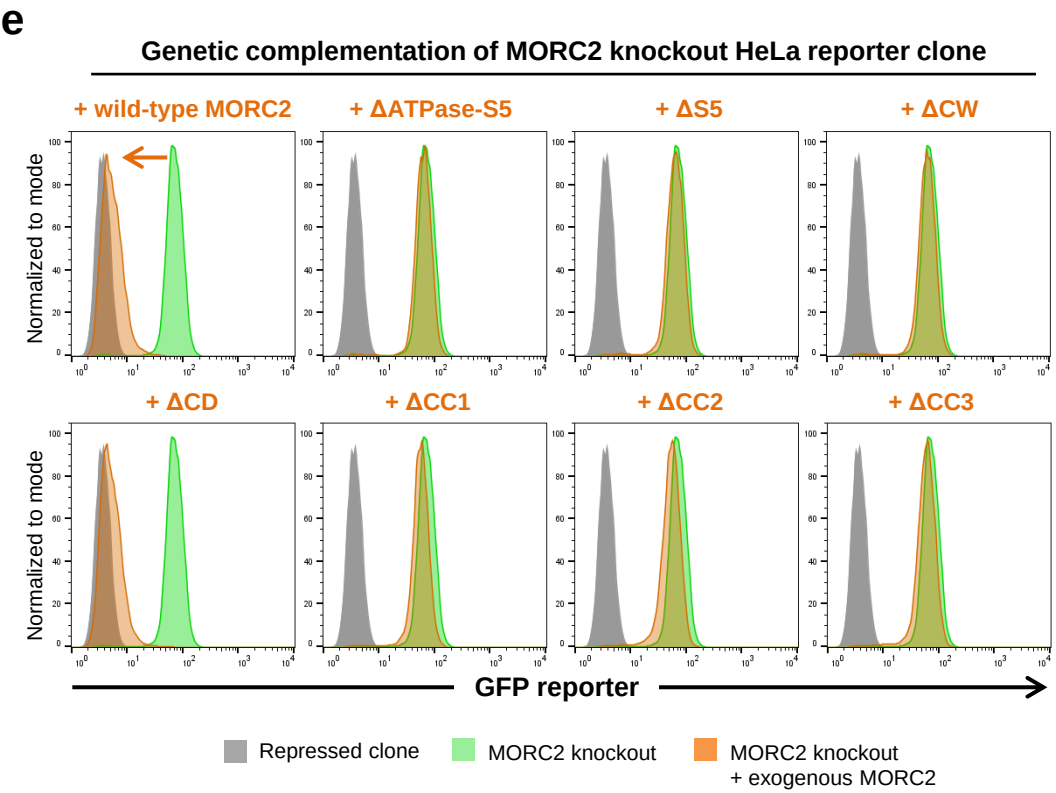
e
Genetic complementation of MORC2 knockout HeLa reporter clone
+ wild-type MORC2
+ ΔATPase-S5
+ ΔS5
+ ΔCW
+ ΔCD
+ ΔCC1
+ ΔCC2
+ ΔCC3
Normalized to mode
GFP reporter
Repressed clone
MORC2 knockout
MORC2 knockout
+ exogenous MORC2

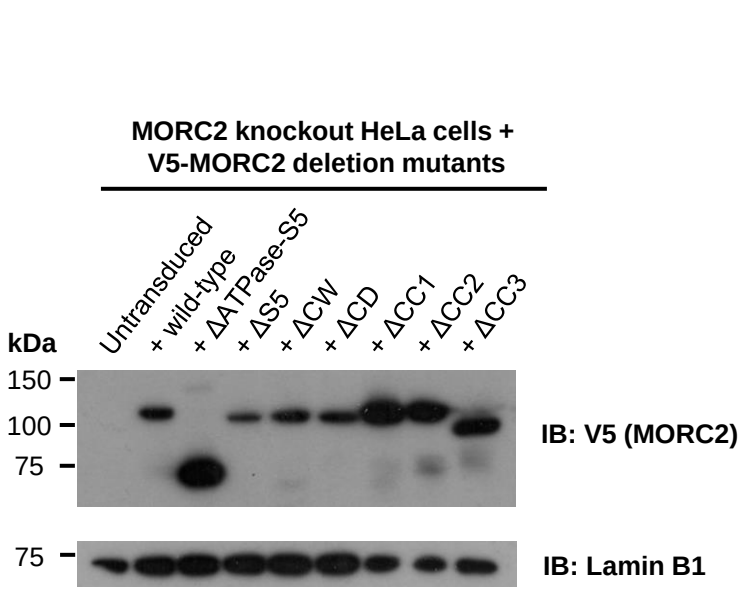
f
MORC2 knockout HeLa cells +
V5-MORC2 deletion mutants
Untransduced
+ wild-type
+ ΔATPase-S5
+ ΔS5
+ ΔCW
+ ΔCD
+ ΔCC1
+ ΔCC2
+ ΔCC3
kDa
150
100
75
75
IB: V5 (MORC2)
IB: Lamin B1

Figure 3

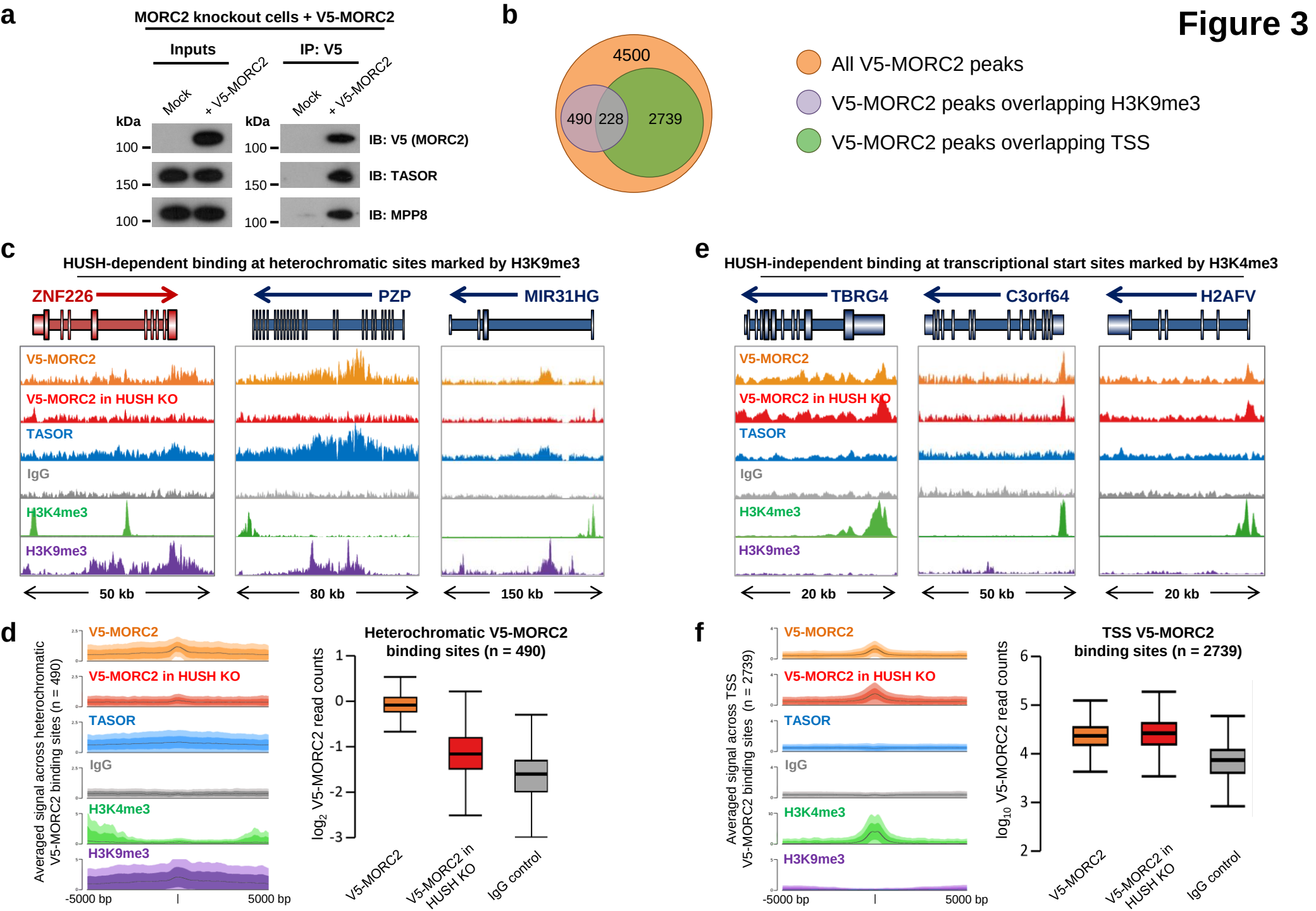
a
MORC2 knockout cells + V5-MORC2
Inputs
IP: V5
Mock
+ V5-MORC2
kDa
100
150
IB: V5 (MORC2)
IB: TASOR
IB: MPP8
b
4500
490
228
2739
All V5-MORC2 peaks
V5-MORC2 peaks overlapping H3K9me3
V5-MORC2 peaks overlapping TSS
c
HUSH-dependent binding at heterochromatic sites marked by H3K9me3
ZNF226
PZP
MIR31HG
V5-MORC2
V5-MORC2 in HUSH KO
TASOR
IgG
H3K4me3
H3K9me3
50 kb
80 kb
150 kb
e
HUSH-independent binding at transcriptional start sites marked by H3K4me3
TBRG4
C3orf64
H2AFV
20 kb
50 kb
20 kb
d
Averaged signal across heterochromatic V5-MORC2 binding sites (n = 490)
-5000 bp
5000 bp
Heterochromatic V5-MORC2 binding sites (n = 490)
log2 V5-MORC2 read counts
V5-MORC2
V5-MORC2 in HUSH KO
IgG control
f
Averaged signal across TSS V5-MORC2 binding sites (n = 2739)
TSS V5-MORC2 binding sites (n = 2739)
log10 V5-MORC2 read counts

Figure 4

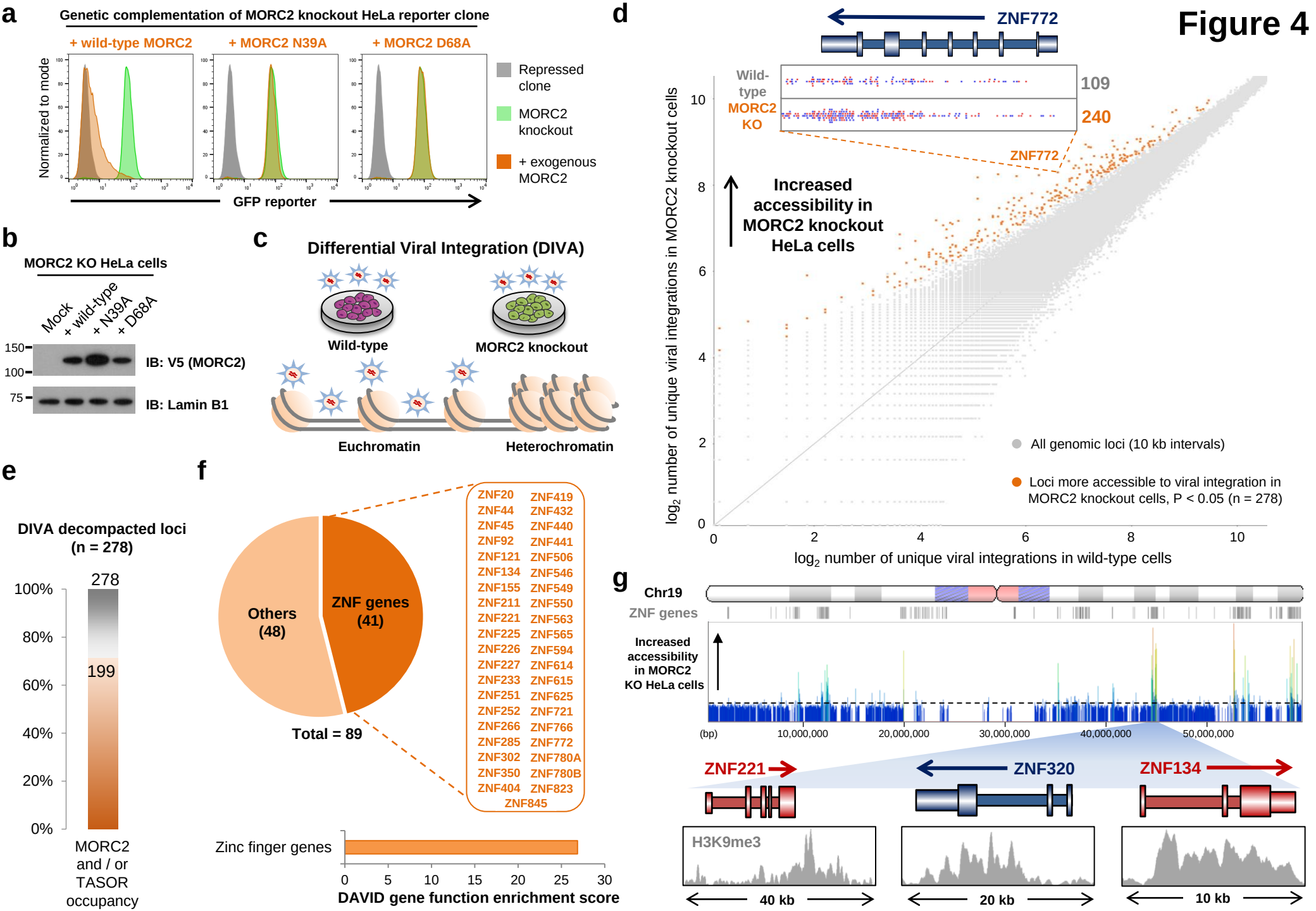
a
Genetic complementation of MORC2 knockout HeLa reporter clone
+ wild-type MORC2
+ MORC2 N39A
+ MORC2 D68A
Normalized to mode
GFP reporter
Repressed clone
MORC2 knockout
+ exogenous MORC2
b
MORC2 KO HeLa cells
Mock
+ wild-type
+ N39A
+ D68A
150
100
75
IB: V5 (MORC2)
IB: Lamin B1
c
Differential Viral Integration (DIVA)
Wild-type
MORC2 knockout
Euchromatin
Heterochromatin
d
ZNF772
Wild-type MORC2 KO
109
240
ZNF772
Increased accessibility in MORC2 knockout HeLa cells
log2 number of unique viral integrations in MORC2 knockout cells
log2 number of unique viral integrations in wild-type cells
All genomic loci (10 kb intervals)
Loci more accessible to viral integration in MORC2 knockout cells, P < 0.05 (n = 278)
e
DIVA decompacted loci (n = 278)
278
199
100%
80%
60%
40%
20%
0%
MORC2 and / or TASOR occupancy
f
Others (48)
ZNF genes (41)
Total = 89
ZNF20 ZNF419
ZNF44 ZNF432
ZNF45 ZNF440
ZNF92 ZNF441
ZNF121 ZNF506
ZNF134 ZNF546
ZNF155 ZNF549
ZNF211 ZNF550
ZNF221 ZNF563
ZNF225 ZNF565
ZNF226 ZNF594
ZNF227 ZNF614
ZNF233 ZNF615
ZNF251 ZNF625
ZNF252 ZNF721
ZNF266 ZNF766
ZNF285 ZNF772
ZNF302 ZNF780A
ZNF350 ZNF780B
ZNF404 ZNF823
ZNF845
Zinc finger genes
DAVID gene function enrichment score
g
Chr19
ZNF genes
Increased accessibility in MORC2 KO HeLa cells
(bp)
ZNF221
ZNF320
ZNF134
H3K9me3
40 kb
20 kb
10 kb

Figure 5

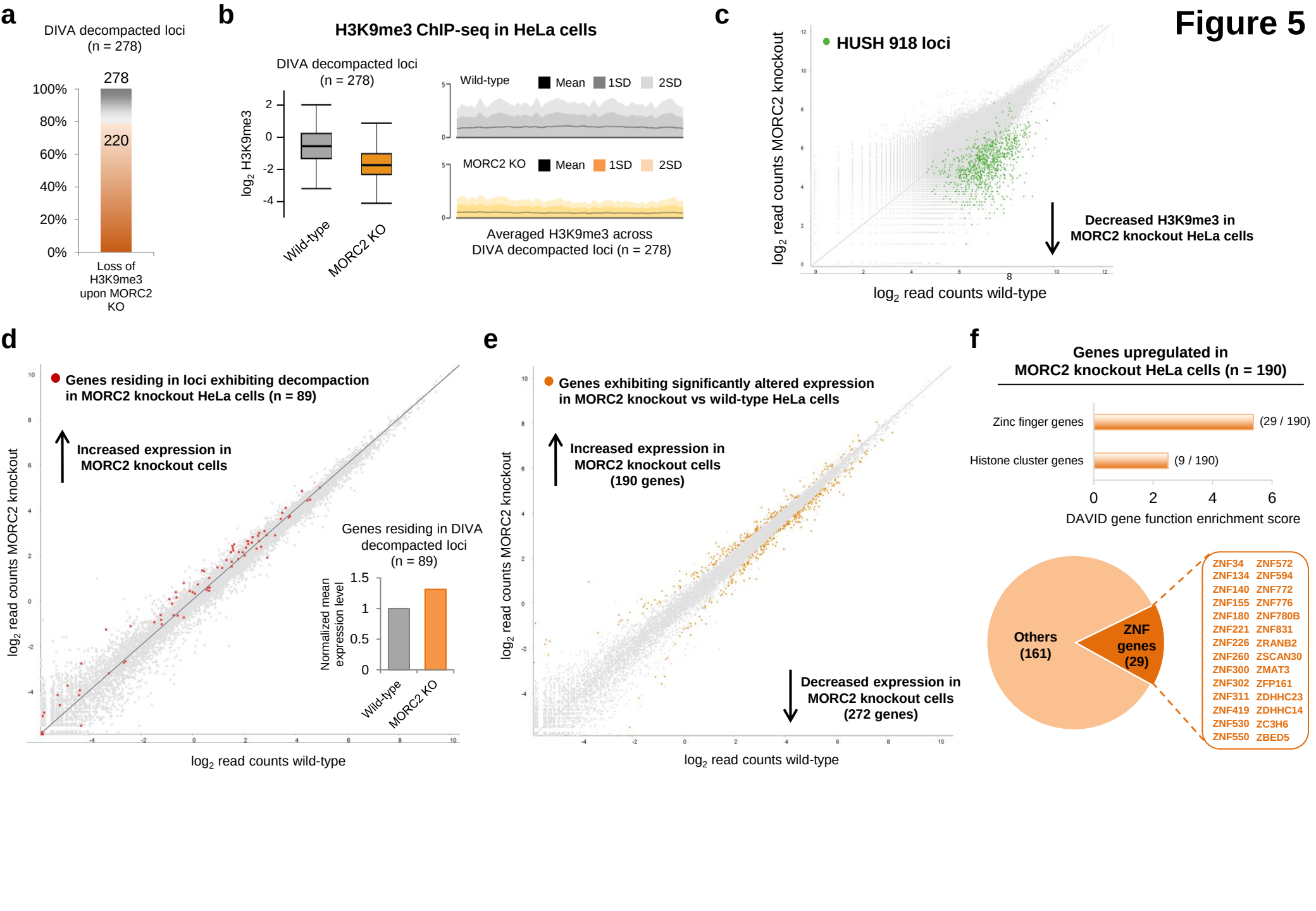
a
DIVA decompacted loci
(n = 278)
278
220
100%
80%
60%
40%
20%
0%
Loss of
H3K9me3
upon MORC2
KO
b
H3K9me3 ChIP-seq in HeLa cells
DIVA decompacted loci
(n = 278)
log2 H3K9me3
Wild-type
MORC2 KO
Wild-type
Mean
1SD
2SD
MORC2 KO
Mean
1SD
2SD
Averaged H3K9me3 across
DIVA decompacted loci (n = 278)
c
HUSH 918 loci
log2 read counts MORC2 knockout
log2 read counts wild-type
Decreased H3K9me3 in
MORC2 knockout HeLa cells
d
Genes residing in loci exhibiting decompaction
in MORC2 knockout HeLa cells (n = 89)
Increased expression in
MORC2 knockout cells
log2 read counts MORC2 knockout
log2 read counts wild-type
Genes residing in DIVA
decompacted loci
(n = 89)
Normalized mean
expression level
Wild-type
MORC2 KO
e
Genes exhibiting significantly altered expression
in MORC2 knockout vs wild-type HeLa cells
Increased expression in
MORC2 knockout cells
(190 genes)
log2 read counts MORC2 knockout
log2 read counts wild-type
Decreased expression in
MORC2 knockout cells
(272 genes)
f
Genes upregulated in
MORC2 knockout HeLa cells (n = 190)
Zinc finger genes
(29 / 190)
Histone cluster genes
(9 / 190)
DAVID gene function enrichment score
Others
(161)
ZNF
genes
(29)
ZNF34
ZNF134
ZNF140
ZNF155
ZNF180
ZNF221
ZNF226
ZNF260
ZNF300
ZNF302
ZNF311
ZNF419
ZNF530
ZNF550
ZNF572
ZNF594
ZNF772
ZNF776
ZNF780B
ZNF831
ZRANB2
ZSCAN30
ZMAT3
ZFP161
ZDHHC23
ZDHHC14
ZC3H6
ZBED5

Figure 6

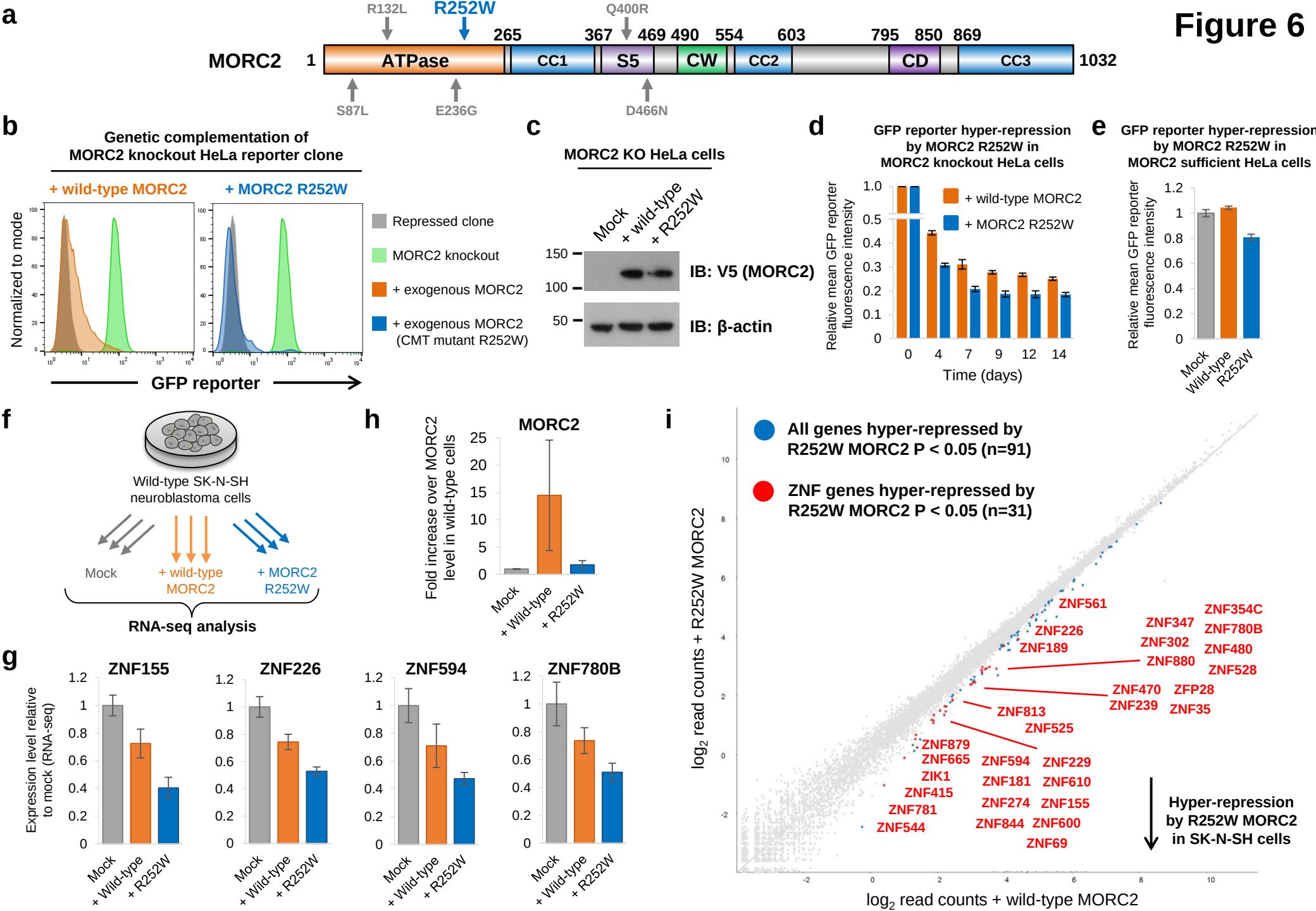
a
R132L
R252W
Q400R
MORC2
1
265
367
469
490
554
603
795
850
869
1032
ATPase
CC1
S5
CW
CC2
CD
CC3
S87L
E236G
D466N
b
Genetic complementation of MORC2 knockout HeLa reporter clone
+ wild-type MORC2
+ MORC2 R252W
Normalized to mode
GFP reporter
Repressed clone
MORC2 knockout
+ exogenous MORC2
+ exogenous MORC2 (CMT mutant R252W)
c
MORC2 KO HeLa cells
Mock
+ wild-type
+ R252W
150
100
50
IB: V5 (MORC2)
IB: β-actin
d
GFP reporter hyper-repression by MORC2 R252W in MORC2 knockout HeLa cells
Relative mean GFP reporter fluorescence intensity
+ wild-type MORC2
+ MORC2 R252W
Time (days)
e
GFP reporter hyper-repression by MORC2 R252W in MORC2 sufficient HeLa cells
Relative mean GFP reporter fluorescence intensity
Mock
Wild-type
R252W
f
Wild-type SK-N-SH neuroblastoma cells
Mock
+ wild-type MORC2
+ MORC2 R252W
RNA-seq analysis
h
MORC2
Fold increase over MORC2 level in wild-type cells
Mock
+ Wild-type
+ R252W
g
ZNF155
ZNF226
ZNF594
ZNF780B
Expression level relative to mock (RNA-seq)
Mock
+ Wild-type
+ R252W
i
All genes hyper-repressed by R252W MORC2 P < 0.05 (n=91)
ZNF genes hyper-repressed by R252W MORC2 P < 0.05 (n=31)
log2 read counts + R252W MORC2
log2 read counts + wild-type MORC2
ZNF561
ZNF226
ZNF189
ZNF347
ZNF354C
ZNF780B
ZNF302
ZNF480
ZNF880
ZNF528
ZNF470
ZFP28
ZNF239
ZNF35
ZNF813
ZNF525
ZNF879
ZNF665
ZNF594
ZNF229
ZIK1
ZNF181
ZNF610
ZNF415
ZNF274
ZNF155
ZNF781
ZNF844
ZNF600
ZNF544
ZNF69
Hyper-repression by R252W MORC2 in SK-N-SH cells

Figure 6

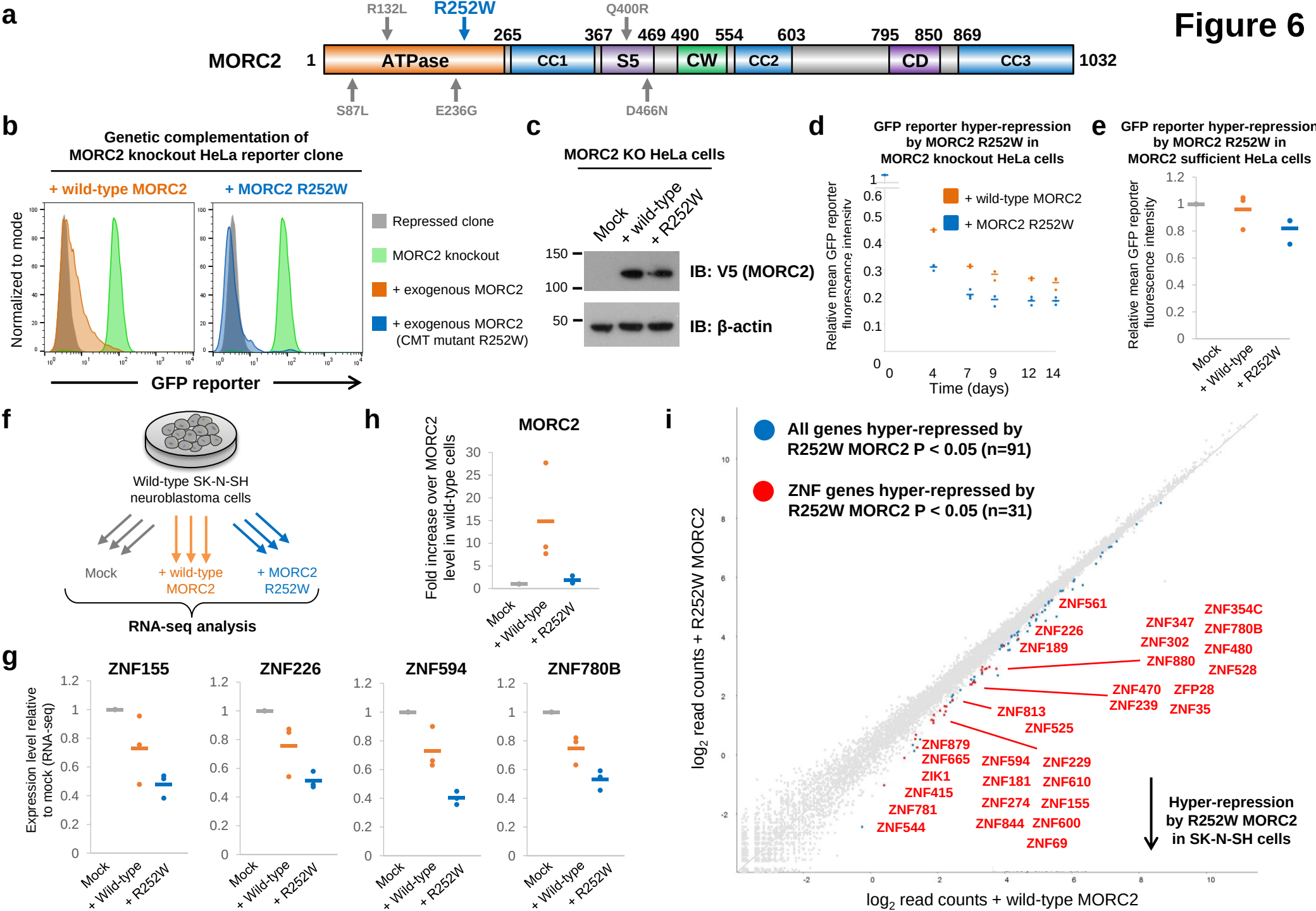
a
R132L
R252W
Q400R
MORC2
1
265
367
469
490
554
603
795
850
869
1032
ATPase
CC1
S5
CW
CC2
CD
CC3
S87L
E236G
D466N
b
Genetic complementation of MORC2 knockout HeLa reporter clone
+ wild-type MORC2
+ MORC2 R252W
Normalized to mode
GFP reporter
Repressed clone
MORC2 knockout
+ exogenous MORC2
+ exogenous MORC2 (CMT mutant R252W)
c
MORC2 KO HeLa cells
Mock
+ wild-type
+ R252W
150
100
50
IB: V5 (MORC2)
IB: β-actin
d
GFP reporter hyper-repression by MORC2 R252W in MORC2 knockout HeLa cells
Relative mean GFP reporter fluorescence intensity
+ wild-type MORC2
+ MORC2 R252W
Time (days)
e
GFP reporter hyper-repression by MORC2 R252W in MORC2 sufficient HeLa cells
Relative mean GFP reporter fluorescence intensity
Mock
+ Wild-type
+ R252W
f
Wild-type SK-N-SH neuroblastoma cells
Mock
+ wild-type MORC2
+ MORC2 R252W
RNA-seq analysis
h
MORC2
Fold increase over MORC2 level in wild-type cells
Mock
+ Wild-type
+ R252W
g
ZNF155
ZNF226
ZNF594
ZNF780B
Expression level relative to mock (RNA-seq)
Mock
+ Wild-type
+ R252W
i
All genes hyper-repressed by R252W MORC2 P < 0.05 (n=91)
ZNF genes hyper-repressed by R252W MORC2 P < 0.05 (n=31)
log2 read counts + R252W MORC2
log2 read counts + wild-type MORC2
ZNF561
ZNF226
ZNF189
ZNF347
ZNF354C
ZNF780B
ZNF302
ZNF480
ZNF880
ZNF528
ZNF470
ZFP28
ZNF239
ZNF35
ZNF813
ZNF525
ZNF879
ZNF665
ZNF594
ZNF229
ZIK1
ZNF181
ZNF610
ZNF415
ZNF274
ZNF155
ZNF781
ZNF844
ZNF600
ZNF544
ZNF69
Hyper-repression by R252W MORC2 in SK-N-SH cells